11-13-2019

Molecular Mechanism of DREAM Dimerization and Interactions with a Non-physiological Ligand Zn2+.

Maria D. Santiago Estevez
msant203@fiu.edu

FLORIDA INTERNATIONAL UNIVERSITY

Miami, Florida

MOLECULAR MECHANISM OF DREAM DIMERIZATION AND INTERACTIONS WITH A NON-PHYSIOLOGICAL LIGAND Zn^{2+}

A thesis submitted in partial fulfillment of the

requirements for the degree of

MASTER OF SCIENCE

in

CHEMISTRY

by

Maria D. Santiago

2019

To: Dean Michael R. Heithaus
College of Arts, Sciences and Education

This dissertation, written by Maria D. Santiago, and entitled Molecular Mechanism of DREAM Dimerization and Interactions with a Non-physiological Ligand Zn^{2+}, having been approved in respect to style and intellectual content, is referred to you for judgment.

We have read this dissertation and recommend that it be approved.

_____
Xiaotang Wang

_____
Francisco Fernandez Lima

_____
Jaroslava Miksovska, Major Professor

Date of Defense: November 13, 2019

The dissertation of Maria D. Santiago is approved.

_____
Dean Michael R. Heithaus
College of Arts, Sciences and Education

_____
Andrés G. Gil
Vice President for Research and Economic Development
and Dean of the University Graduate School

Florida International University, 2019

DEDICATION

To my mother Felicia Estevez and sisters Maria Jose Santiago and Maria Daniel Santiago

who push me to be a better person every day.

ACKNOWLEDGMENTS

I want to thank the Lord Jesus Christ for putting all these beautiful amazing people in my life, each one of them is a blessing and have made me a better person.

Firstly, I would like to acknowledge my advisor and mentor Dr. Jaroslava Miksovska, her support and guidance have been crucial at every moment; none of this thesis or any graduate degree would have been possible without her. She took a chance on me and has been fighting every obstacle by my side since the beginning. I will always be eternally grateful for her commitment as a mentor and as an exceptional human being.

I would also like to acknowledge my committee members Dr. Xiaotang Wang and Dr. Francisco Fernadez-Lima, their kindness and feedback has been greatly appreciated through these two years.

I want to thank my lab partners and friends for their help and support in the lab. Dr. Antonija Tangar, Ruipeng Lei, Samiol Azam, Tetyana Shvets , Adriana Riveron, Sasha Rodriguez, Setareh Sakhdari, Israel Castillo, Joana Almeida, Claribel Utria, Maria Isabel Frias, and Magali Autie. I want to thank my friends Haydee Linares Rosales, Tumpa Dasgupta Carolina Pastorelli and Yoniel Olivares for their emotional support and for giving friendship its true meaning.

I am indebted to my mother Felicia Estevez who has shown me to never give up on anything and has been the reason I always keep moving forward. My sisters Maria Jose Santiago and Maria Daniel Santiago who has been the greatest support and infinite help

since I can remember, they are my biggest blessing; everything is possible with them by my side.

Lastly, I am thankful to the BD Fellowship who provided the financial support during these two years, Dr. Sonja Montas –Hunter and Dr. Alla Mirzoyan who have shown me kindness and support since the beginning.

ABSTRACT OF THE THESIS

MOLECULAR MECHANISM OF DREAM DIMERIZATION AND INTERACTIONS WITH A NON-PHYSIOLOGICAL LIGAND Zn^2+

by

Maria D. Santiago

Florida International University, 2019

Miami, Florida

Professor Jaroslava Miksovska, Major Professor

Downstream Regulatory Element Antagonist Modulator (DREAM) belongs to the family of neuronal calcium sensor proteins and it is involved in several processes in the brain. Zinc has been shown to bind to recoverin, with submillimolar affinity. Based on the high sequence homology between the NCS family, it is proposed that DREAM can also serve as an intracellular target for Zn^{2+}. Fluorescence and CD studies confirm that zinc binds to DREAM with a of K_d = 4 μM, triggering changes in the proteins' tertiary structure. The calcium association to DREAM leads to the formation of a Ca^{2+} bound dimer, while in the apo state, a monomer-tetramer equilibrium was observed. A chimeric version of DREAM was prepared by mutating the residues involved in dimerization. DREAM-NCS1 properties were investigated using spectroscopic techniques. These results point towards the role of hydrophobic interactions and salt bridges in stabilizing the dimer and propagating allosteric signals.

TABLE OF CONTENTS

CHAPTER PAGE

LIST OF TABLES

TABLE PAGE

LIST OF FIGURES

FIGURE PAGE

LIST OF ABREVIATIONS

ABBREVIATION	FULL NAME
1,8-ANS	1-anilinonaphthalene-8-sulfonic acid
ΔH	Enthalpy change
ΔS	Entropy change
λ_{max}	Emission maxima
Ca^{2+}	Calcium
CaM	calmodulin
CD	Circular dichroism
DREAM	Downstream regulatory element antagonist modulator 2-
EDTA	({2-[Bis(carboxymethyl)amino]ethyl} (carboxymethyl)amino)acetic acid
EFX	EF-hand X
EGTA	ethylene glycol-bis(2-aminoethylether)-N,N,N′,N′-tetraacetic
IPTG	Isopropyl β-D-1-thiogalactopyranoside
KChIP	Potassium channel interaction protein
Kd	Dissociation constant
Mg^{2+}	Magnesium
TRIS	2-Amino-2-hydroxymethyl-propane-1,3-diol

1. INTRODUCTION

1.1 Ca^{2+} storage and functions.

Calcium is an intracellular messenger, which is involved in several processes such as neurotransmitter release, muscle contraction, and gene expression modulation. All these processes are regulated by the spatial and temporal location of Ca^{2+} (Lock, Smith, & Parker, 2019) (Fig.ure 1.1). The intracellular Ca^{2+} concentration is around 10^{-8} M and it is maintained by Ca^{2+}-ATPase pumps and Na^{+}/Ca^{2+} exchange, as well as sequestering in organelles such as the endosome, the Golgi apparatus, and the endoplasmic reticulum (Permyakov, E. A. & Kretsinger, 2011). Intracellularly, the concentration of Ca^{2+} ions is regulated by ligand-gated Ca^{2+} channels. Calcium is released in the ER by inositol triphosphate (IP3) receptor linked channels and ryanodine receptors. In IP3 signaling, phospholipase c, activated through the GPCR pathway, cleaves phosphatidylinositol bisphosphate into IP3, which binds to IP3 receptors resulting in the release of Ca^{2+} from the ER. It is worth mentioning that IP3 signaling requires the co-stimulation of Ca^{2+} resulting in Ca^{2+} induced-Ca^{2+} release mechanism (Lock et al., 2019) . Secondly, ryanodine receptors can also be activated by molecules such as caffeine and stimulate Ca^{2+} release (Permyakov, E. A. & Kretsinger, 2011). In excitable cells such as neurons, the concentration of Ca^{2+} is mainly regulated by voltage gated Ca^{2+} channels. When the membrane potential of the neurons is between -60 to -70 mV, the voltage gated Ca^{2+} channels are closed and the cell is in a resting state. On the other hand, when specific channels are activated Ca^{2+} enters the cell resulting in neuronal excitation (Ramirez, Gonzalez, Fissore, & Carvacho, 2017).

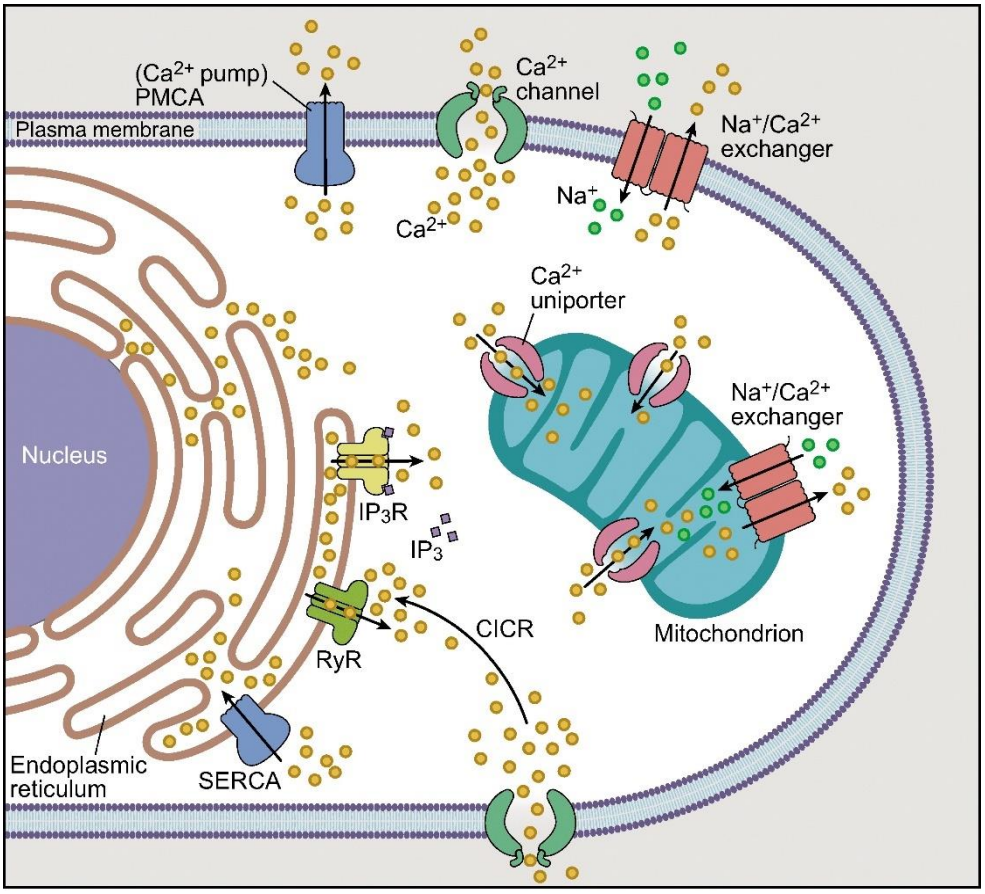

Fig. 1.1: Processes that control Ca^{2+} storage and release in the eukaryotic cell (Dong, Saikumar, Weinberg, & Venkatachalam, 2006)

1.2 Calcium binding proteins

Calcium binding proteins (CBP) are traditionally divided into two groups, Ca^{2+} buffers and Ca^{2+} sensors (Permyakov & Kretsinger, 2011). Calcium buffer proteins such as parvalbumin and calbildin are able to regulate intracellular Ca^{2+} concentration by binding to the metal and participating in signal transduction (Permyakov & Kretsinger, 2011) . On the other hand, Ca^{2+} sensors undergo conformational changes upon Ca^{2+} binding, which ultimately modulate their affinity for intracellular partners. (Permyakov & Kretsinger, 2011)

1.2 Calmodulin as a model protein for EF-hands calcium sensors

The study of calmodulin has provided a model for the members of the EF-hands calcium sensors. Calmodulin is present in all eukaryotic cells (Permyakov & Kretsinger, 2011) and it has been conserved during evolution because of its interactions with several partners in Ca^{2+} signal transduction pathways (Permyakov & Kretsinger, 2011). The protein possesses 4 EF-hands and it is involved in several signal transduction pathways (Chazin, 2011; Permyakov & Kretsinger, 2011). Calmodulin transduces the calcium signal by binding to Ca^{2+}, which triggers a conformational change resulting in a less compact structure than the one in the apo form with exposed hydrophobic patches on the protein surface as shown in Fig. 1.2 , allowing Ca^{2+} bound calmodulin to bind to the final target of the signaling pathway (Permyakov, E. A. & Kretsinger, 2011).

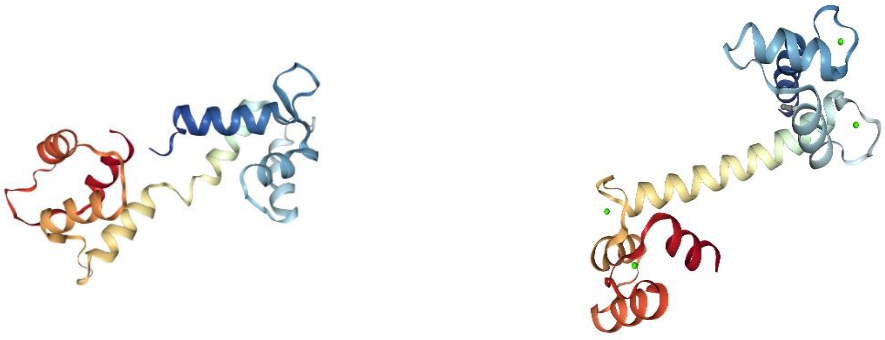

Fig. 1.2: Structure of Apo Calmodulin (PDB entry 1CFD) . Structure of Ca^{2+}-Calmodulin (PDB entry 1CLL)

The most significant Ca^{2+} induced change in calmodulin is the change in the orientation of the helixes for each EF hand (Permyakov, E. A. & Kretsinger, 2011). In the apo form, the first and last helixes are parallel to the central helix linker shown in Fig. 1.2, forming a compact hydrophobic core (Permyakov, E. A. & Kretsinger, 2011). In the Ca^{2+} bound calmodulin, these helixes move away from the central helix linker, resulting in a change in the orientation with respect to the central helix linker, from 121-144 ° in the apo form to 86-116° in the Ca^{2+} bound calmodulin (Permyakov & Kretsinger, 2011). This observed reorientation upon Ca^{2+} binding produces a solvent exposure of methionine residues and concomitant formation of two hydrophobic concave patches that serve as binding sites for the intracellular partners (Permyakov & Kretsinger, 2011).

1.3 Calcium coordination and- binding site in EF –hand proteins

The calcium-binding site in EF-hand proteins is formed by a helix-loop-helix structure where Ca^{2+} is coordinated to the protein in a pentagonal bipyramidal geometry as shown in Fig. 1.3 (Gifford, Walsh, & Vogel, 2007). The helix-loop-helix is formed by an α-helix, a Ca^{2+} binding loop composed of nine residues, and an additional α-helix composed of eleven residues.(Gifford et al., 2007). The nine residues in the Ca^{2+} binding loop provide five ligands for Ca^{2+} coordination and two extra ligands are provided by the side chain of a Glu residue, resulting in the seven ligands that coordinate Ca^{2+} in the EF-loop (Gifford et al., 2007). In addition, a water molecule forming hydrogen bonds with one of the side chains of the loop completes the coordination sphere of Ca^{2+}(Gifford et al., 2007). These EF-loops are mostly composed of negatively charged amino acids Asp and Glu (Gifford et al., 2007), reflecting the preference of the EF-loop for less bulky carboxy side chains as

shown in Table 1.1 (Gifford et al., 2007). The coordination of Ca^{2+} bound to EF-hand 3 and EF-hand 4 is shown in Fig. 1.4.

Table 1.1: Sequence of amino acid residues in canonical calcium binding loop. Adapted from (Gifford et al., 2007)

EF-loop position	1	2	3	4	5	6	7	8	9	10	11	12
coordinating ligand	X		Y		Z		-Y		-X			-Z
Most common	Asp 100 %	Lys 29 %	Asp 76 %	Gly 56 %	Asp 76 %	Gly 96 %	Thr 23 %	Ile 68 %	Asp 32 %	Phe 23 %	Glu 29 %	Glu 92 %
Also frequently observed		Ala Gln Thr Val Ile Ser Glu Arg	Asn	Lys Arg Asn	Asn		Phe Lys Gln Tyr Glu Arg	Val Leu	Ser Thr Glu Asn Gly Gln	Tyr Ala Thr Leu Glu Lys	Asp Lys Ala Pro Asn	Asp

Fig. 1.3: Ca^{2+} coordination by the canonical EF-hand illustrating the pentagonal bipyramidal coordination of the Ca^{2+} ion (continuous thin lines) and the hydrogen bonding pattern in the loop (dashed lines) . The backbone NH groups are shown in black, the side-chain oxygen atoms in red, the Ca^{2+} ion in yellow and the coordinating water molecule in blue (Gifford et al., 2007).

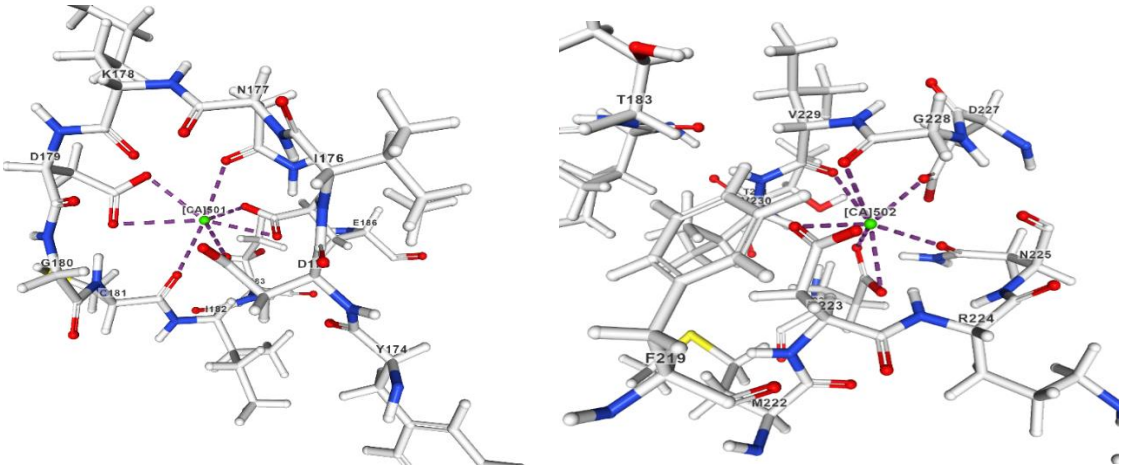

Fig. 1.4: Calcium coordination in EF-hand 3 (A) and EF-hand 4 (B) of neuronal calcium sensor DREAM, (PDB entry 2JUL).

1.4 Ca^{2+} and neuronal calcium sensors in the brain

The concentration of Ca^{2+} ions plays a crucial role in neuronal activity (Burgoyne & Weiss, 2001), since it modulates several processes such as neurotransmitter release, short term

rapid modulations of channel function, long-term switches in gene expression (Burgoyne & Weiss, 2001), regulation of Kv4.3 and Kv1.5 potassium channels, and regulation of presenilin processing (Pongs et al., 1993). The ability of Ca^{2+} to regulate such a variety of processes is due to its interactions with numerous CPBs, which associate with other target proteins involved in the process mentioned before. (Burgoyne, R. D. & Weiss, 2001)

1.5 Neuronal Calcium Sensors.

Neuronal calcium sensors (NCS) are expressed in retinal photoreceptors (Burgoyne & Weiss, 2001) and in the brain (Burgoyne & Weiss, 2001; Permyakov & Kretsinger, 2011). The family of proteins is in charge of regulating a variety of physiological processes summarized in Fig. 1.5 and are linked to several pathological conditions such as Parkinson, Huntington and Alzheimer's disease (López-Hurtado et al., 2018). The family is composed of five different classes: A,B,C,D, and E referring to frequenin, visinin-like protein (VILIP), recoverins, guanylate cyclase (GC)-activating proteins (GCAPs), and Kv-channel-interacting proteins (KChIPs) (Burgoyne, R. D. & Weiss, 2001). The main characteristics of the protein family are a tandem-like structural orientation of the N- and C- terminal domain and posttranslational myristoylation of the N- terminal residue. In addition, the sequence of the N- terminal domain shows a low sequence similarity, whereas

the C- terminal domain sequence is homologous among the members of this family. (Permyakov. & Kretsinger, 2011).

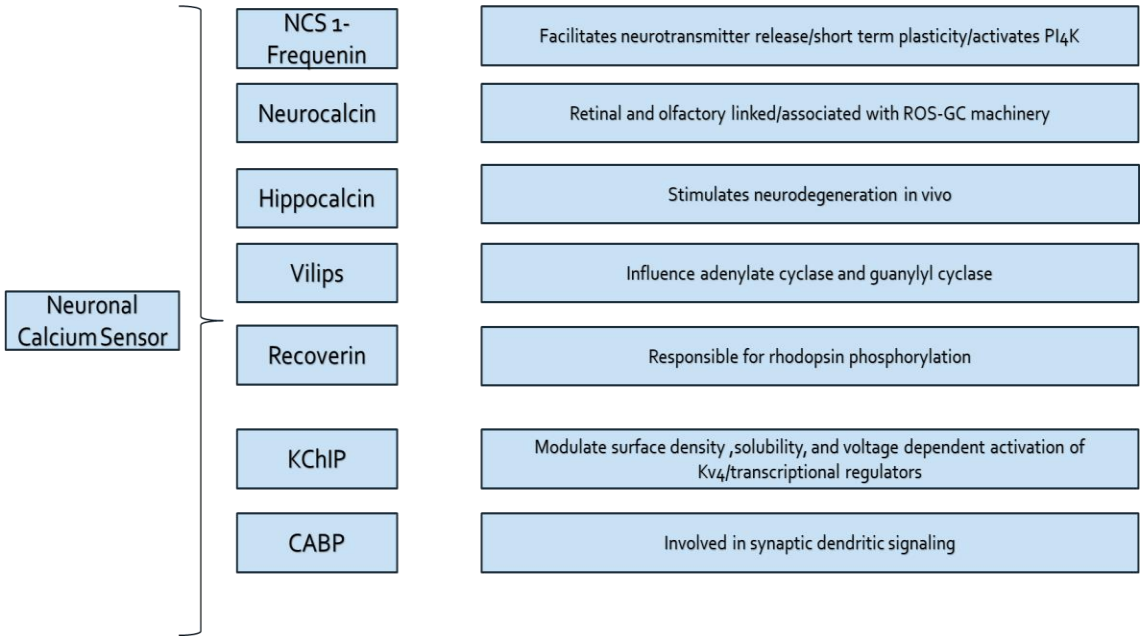

Fig. 1.5: Neuronal Calcium Sensor subfamilies classifications and main function Adapted from (Permyakov, E. A. & Kretsinger, 2011)

Class A , frequenin (NCS-1), first appeared in yeast (Burgoyne & Weiss, 2001) and it can bind up to three Ca^{2+} ions (Ames & Lim, 2012) and a myristoyl group can be found at the N terminal allowing the protein to associate with lipid layers (Braunewell, Karl-Heinz & Gundelfinger, 1999; Dason, Romero-Pozuelo, Atwood, & Ferrús, 2012) . Class B, VILIPs, is formed by three members VILIP 1, 2 and 3. Visinin like proteins play a role in the regulation of the desensitization of signal cascades in retinal photoreceptors in a Ca^{2+} depended manner (Braunewell, Spilker, Behnisch, & Gundelfinger, 1997). Class C is formed by one protein, recoverin, which has one human gene (Burgoyne & Weiss, 2001).

Recoverin is present in photoreceptor cells and its main function is to control light sensitivity by regulating the phosphorylation of rhodopsin kinase (Calvert, Klenchin, & Bownds, 1995). Furthermore, as in the case of NCS-1, recoverin interacts with a myristoil group, which is responsible for inducing rhodopsin kinase inhibition in Ca^{2+} dependent manner (Calvert et al., 1995). Class D is formed by GCAPs 1, 2 and 3 (Burgoyne & Weiss, 2001) and is expressed in the photoreceptors cells in the retina (Braunewell, Karl-Heinz & Gundelfinger, 1999). The main function of GCAPs is to activate or inhibit guanylyl cyclase in the retina (Burgoyne, Robert D. & Haynes, 2012). Class E is formed by KChIP 1, 2 and 3 (Burgoyne, R. D. & Weiss, 2001). They interact with the Kv4 family of A-type potassium channels (Burgoyne & Haynes, 2012) and may participate in regulating voltage-gated Ca^{2+} channel signaling (Burgoyne & Haynes, 2012) . The KChIP 1-4 family bind with the cytosolic α-subunit of potassium channels, so called T1 domain (Ling et al., 2000), forming a cross-shaped octamer (Findeisen, Hura, Minor, & Pioletti, 2006), Pioletti *et al*. determined an X-ray structure of KChIP1 in complex with potassium channel showing that each KChIP1 monomer interacts with two Kv4.3 T1 domains, forming an octamer which is composed by four KChIP1s and four Kv4.3 subunits. (Findeisen et al., 2006), The first KCHIP1- Kv4.3 binding site is formed by hydrophobic interactions among the hydrophobic residues in the N terminal of Kv4.3 and a hydrophobic cavity on the surface of KChIP1, so called Site 1 is composed of amino acids 2-22 from Kv4.3. The second binding site is between the N terminal of KChIP1 and a T1 domain loop, so called Site 2, and corresponds to amino acids 70-90 from the T1 domain (Findeisen et al., 2006). The class E member KChIP 2 is present in cardiomyocytes and it has been proposed to interact with presenilin and have a role in the ryanodine receptor-mediated Ca^{2+}-induced

Ca^{2+} release (Bähring, 2018). The third class E member, KChIP3 also known as DREAM or calsenilin interacts with DNA and regulates gene expression of genes involved in pain sensing such prodynorphin gene; it activates presenilin, and modulates kinetics of Kv channels through interactions with the T1 domain. (Burgoyne, Robert D. & Haynes, 2012).

1.6 Downstream Regulatory Element Antagonist Modulator.

Downstream Regulatory Element Antagonist Modulator (DREAM) is a member of the NCS family, which belongs to the potassium voltage channel subfamily (Carrión, Link, Ledo, Mellström, & Naranjo, 1999). The DREAM protein is composed of 256 amino acids and contains 4 EF hands as shown in Fig. 1.6. and 1.7. The EF hand 1 does not bind any metal due to the presence of a proline residue within the metal binding loop, EF hand 2 binds to Mg^{2+} with an equilibrium dissociation constant of around 13 μM (Masanori Osawa et al., 2005), and EF hand 3 and 4 bind to Ca^{2+} with an affinity of around 1 μM (Masanori Osawa et al., 2005). DREAM also interacts with small hydrophobic molecules such as 1,8 ANS and arachidonic acid with an affinity modulated by Ca^{2+} binding to the protein. (Gonzalez & Miksovska, 2014). The NMR structure of the truncated form (residue 76 to 256) of Ca^{2+} bound DREAM is shown in Fig. 1.6. Ten α-helix were identified in the truncated form with helices 2-5 forming EF-hand 1 and EF-hand 2 and helices 6-9 forming EF-hand 3 and EF-hand 4. (Lusin, Vanarotti, Li, Valiveti, & Ames, 2008).

Previous studies have shown that DREAM is involved in several biological processes. Ooi *et al.*(2008*)* have shown that DREAM is able to regulate learning and memory by inhibiting the activity of cAMP Response Element Binding Protein (CREB). In the absence of Ca^{2+}, DREAM binds to DRE sequence, inhibiting the expression of genes regulated by CREB/CREM complex. In the presence of Ca^{2+}, DREAM dissociates from DNA allowing

the expression of CREB/CREM genes (Ooi & Wood, 2008) . Furthermore, in the absence of Ca^{2+}, DREAM interacts with CREB and CREM (cAMP Response Element Modulator) inhibiting cAMP-mediated transcriptional activation (Ooi & Wood, 2008).

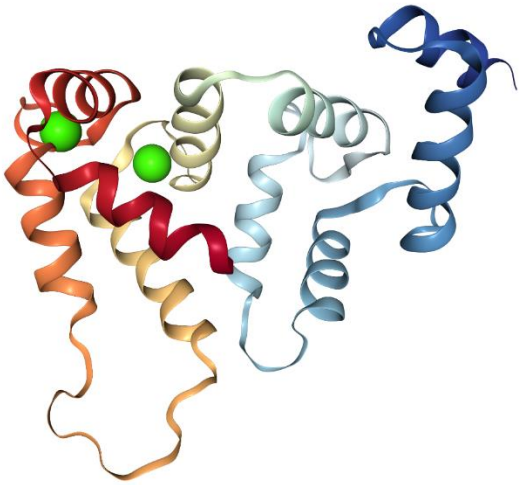

Fig. 1.6: DREAM structure determined by NMR. α-helices are shown as ribbons with the N-terminal domain shown in blue and the C-terminal domain in red, Ca^{2+} ions are represented as green spheres. (PDB entry 2JUL)

```
        10         20         30         40         50         60
MQRTKEAVKA SDGNLLGDPG RIPLSKRESI KWQRPRFTRQ ALMRCCLIKW ILSSAAPQGS

        70         80         90        100        110        120
DSSDSELELS TVRHQPEGLD QLQAQTKFTK KELQSLYRGF KNECPTGLVD EDTFKLIYSQ

       130        140        150        160        170        180
FFPQGDATTY AHFLFNAFDA DGNGAIHFED FVVGLSILLR GTVHEKLKWA FNLYDINKDG

       190        200        210        220        230        240
CITKEEMLAI MKSIYDMMGR HTYPILREDA PLEHVERFFQ KMDRNQDGVV TIDEFLETCQ

       250
KDENIMNSMQ LFENVI

EF 1 EF 2 EF 3 EF 4
```

Fig. 1.7: Amino acid sequence of DREAM. The sequence corresponding to the individual EF-hands is shown in green, red, blue and yellow.

Furthermore, the binding of DREAM to DRE sequence is also involved in the transcriptional repression of prodynorphin genes related to pain sensitivity and c-fos, c-junk, and hrk genes related to cell proliferation. This ability of DREAM to bind to DNA makes it the only known CBP to regulate gene expression in a calcium dependent manner (Carrión et al., 1999; Cheng & Penninger, 2004).

The DREAM protein like all members of KChIP proteins, modulates A-type potassium currents by interacting with Kv4.3 potassium channels (Ling et al., 2000). Even though the structure for KChIP1 in complex with potassium voltage channel is the only that has been determined (Findeisen et al., 2006), the KChIP family has a high sequence similarity and the amino acids involved in the stabilization of the KCHIP1-Kv4.3 interactions are conserved throughout the KChIP family (Ling et al., 2000). Therefore, analogous interactions are expected between all KChIPs and potassium voltage channels.

The importance of DREAM in neurological and neuropathological processes is clearly demonstrated by the fact that DREAM is implicated in several neurological diseases such as Alzheimer's disease, Huntington and Parkinson disease (López-Hurtado et al., 2018). Lilliehook *et al.* (1998) reported that DREAM interacts with the presenilin unit of the γ-secretase complex and enhances the cleavage of amyloid precursor proteins into aβ42 plaques. The plaques are commonly found post-mortem as a diagnostic feature of patients with Alzheimer's disease (Lilliehook et al., 1998).

The precise mechanism of how Ca^{2+} modulates DREAM interaction with DNA and other intracellular partner remains unknown. This protein has been shown to undergo an oligomerization transition upon binding of Ca^{2+} (Masanori Osawa et al., 2005; Yu et al., 2007). In the absence of Ca^{2+}, DREAM presents a monomer-tetramer equilibrium whereas

upon Ca^{2+} binding to the C- terminal domain, the protein forms a stable dimer (Carrión et al., 1999; Gonzalez & Miksovska, 2014; Lusin et al., 2008). Previous studies have shown that DREAM interacts with potassium channels as a monomer (Ping Liang et al., 2009; Yu et al., 2007) in both the Ca^{2+} bound and Ca^{2+} free form, with presenilin and calmodulin as a dimer, and with DNA as a monomer or tetramer (Carrión et al., 1999) suggesting that changes in the protein oligomerization are important for Ca^{2+} signaling mechanism.

1.7 Objectives

Objective 1:

Zinc is a divalent cation, which possesses a filled d orbital, which means that it does not participate in redox reaction. Because of this Zn^{2+} can be used as a cofactor in biological reaction which do not required the presence of a metal, which can be involved in redox reactions [JM1]

Previous studies have shown that Zn^{2+} is able to bind to Ca^{2+} buffer proteins such as parvalbumin with a Kd of $5x10^{-5}$ M. (Permyakov, E. A. & Kretsinger, 2011) Furthermore, Zn^{2+} is also able to bind to calmodulin albeit weakly with a dissociation constant od 10^{-3} M (Warren, Guo, & Tang, 2007). The metal binding site in proteins, which bind to Zn^{2+} usually, involve His Glu Asp and Cys. Some of the biological functions of Zn^{2+} involve neuronal growth and plasticity indicating a similar role as that of Ca^{2+}. Recently[JM2] published study by Permyakov *et al*. have shown that Zn^{2+} binds to a member of neuronal calcium sensor family, recoverin with an affinity of 7.0 μM (Permyakov, S. E. et al., 2003). Considering a high sequence and structural homology between members of NCS family, it is proposed that DREAM can also serve as an intracellular target for Zn^{2+}. With this in

mind, we conducted fluorescence studies and circular dichroism studies to elucidate zinc binding to DREAM and its impact on protein stability.

Objective 2:

Even though results from several research groups have addressed structural and functional properties of DREAM, the molecular mechanism of calcium triggered signaling and allosteric regulation with intracellular partners remains unknown for DREAM and other members of the neuronal calcium sensor family. The goal of my thesis was to provide insight into the Ca^{2+} triggered dimerization process of DREAM. Considering the high sequence homology of the C- terminal domain among neuronal calcium sensors, the results obtained in my study can be applied to other potassium channel interacting proteins and other members of the neuronal calcium sensor family.

Previous studies by the Ames group suggested that hydrophobic interactions between Leu residues (Leu155, Leu159 and Leu251) stabilize the dimeric form of the Ca^{2+} bound DREAM dimer. However, the unpublished computational and polarization data from our group indicate that two salt bridges between individual monomers (Arg 200, Arg 207, and Glu 103) also contribute to the protein stability. To study the DREAM dimerization mechanism, we designed a chimeric DREAM-NCS 1 protein. Taking into account that the NCS1 protein does not form a dimer in the Ca^{2+} bound form, we have replaced residues in the loop connecting EF-hand 3 and EF-hand 4 with the sequence found in NCS1. In addition, hydrophobic residues Leu 157 and Leu 158 have been replaced by alanine residue corresponding to the analogues residues in neuronal calcium sensor 1 (Thr 157 and Ser

158) which does not form dimers. The alignment of the sequence of DREAM WT and DREAM-NCS1 chimeric protein is shown in Figure 1.8. The structural properties of the chimeric protein were investigated using steady state and time resolved fluorescence and circular dichroism spectroscopy. In addition, interaction of the chimeric protein with the peptides mimicking the DREAM binding sites in T1 domain of Kv channel were characterized.

2. MATERIALS AND METHODS

2.1 Chemicals and reagents

Reagents and solvents $CaCl_2$, ZnCl2, $MgCl_2$, EDTA and EGTA, as well as the reagents required for the protein expression and purification were purchased from Sigma-Aldrich or Fischer Scientific and were of analytical grade. The hydrophobic fluorescent probe 1,8-ANS, was purchased from Invitrogen. 1,8-ANS, stock was prepared in ultrapure water (18.2 MΩ) and stored at -20°C and the concentration was determined spectrophometrically using the extinctions coefficients listed in Table 2.1.

Fluorescently labeled peptides Site 1 and Site 2 were purchased from Thinkpeptides, the stocks were prepared in 20 mM Tris buffer pH 7.4 and the concentration was determined spectrophotometrically using the extinction coefficients listed in Table 2.1.

2.2 Protein purification and isolation.

Recombinant mouse DREAM (65-256) protein with a His tag at the N-terminus was expressed in *E. coli* (DE 21) (Invitrogen). Cells were grown in Terrific Broth (TB) media at 37ºC and 250 rpm speed for 12 h. Isopropyl β-D-1-thiogalactopyranoside (IPTG) was added when optical density at 600 nm (OD) reached 0.75 and cells were grown for additional 12 h. Subsequently, cells were harvested by centrifugation at 4 °C and 5000 rpm for 20 min (ST 16R centrifuge, Thermal Scientific) and treated with lysis buffer overnight. The composition of the lysis buffer is 20 mM Tris-HCl, pH 8.0, 300 mM NaCl, 1 mM β-mercaptoethanol, 20% glycerol, 1mM phenylmethyl sulfonyl fluoride (PMSF), 0.2%

Tween 20, 20 μg/mL DNase I, 5 μg/mL lysozyme, and 5 mM $MgCl_2$ and pH 8.0 . Cells were broken through sonication using a sonic dismembrator (model 100, Fisher Scientific) for 40 intervals of 20 seconds with 2 min of resting on ice between each interval. Disrupted cells were centrifuged for 4 hours at 5000 rpm and supernatant was collected. Supernatant was then passed through a Ni-NTA affinity column (Quiagen) equilibrated with buffer A containing 20 mM Tris-HCl, pH 8.0, 300 mM NaCl, 1 mM β-mercaptoethanol, and 10% glycerol. The column was washed with an increasing concentration of imidazole in buffer A (10 mM , 20 mM and 40 mM) until the OD of the eluate at 280 was less than 0.02. Finally, and the protein was eluted with buffer A containing 250 mM imidazole. Protein was then dialyzed against a 20 mM Tris buffer pH 8.0 to remove residual imidazole and passed through an anion exchanged di-ethyl-amino-ethyl (DEAE) column, which was consecutively washed with 20 mM Tris buffer pH 8.0 containing an increasing NaCl concentration (20 mM ,40 mM , and 80 mM NaCl). The protein was eluted with 200 mM NaCl in 20 mM Tris buffer pH 8.0 and dialyzed against 20 mM TRIS pH 7.4 overnight. The purity of the protein was determined using SDS-PAGE electrophoresis and the Ca^{2+} binding properties were characterized using emission spectroscopy and circular dichroism spectroscopy as described below.

2.3 UV-VIS absorption

The presence of aromatic amino acid residues with conjugated electrons, Trp, Phe and Tyr, peptides and proteins the ability to absorb light in the UV range from 250 nm to 300 nm.

These conjugated systems allow to observe π ->π* electronic transitions upon excitation as shown in the Jablonski diagram (Figure 2.1)

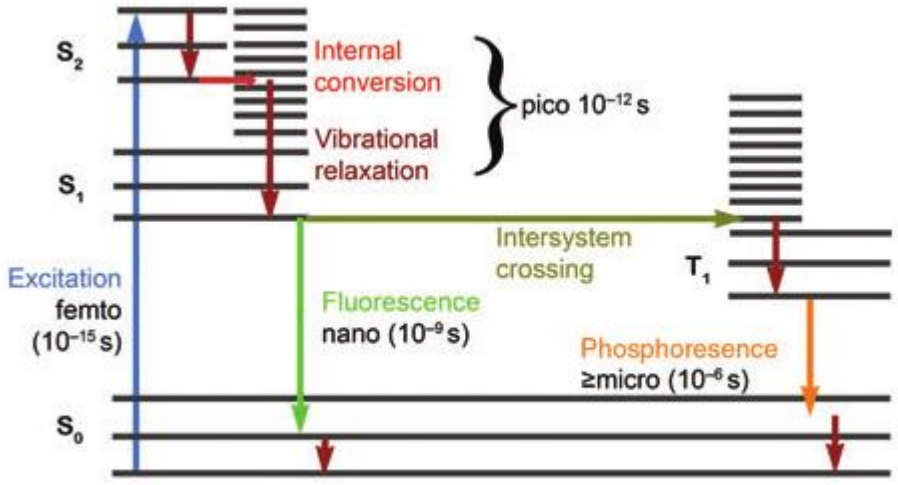

Fig. 2.1: Representation of the Perrin-Jablonski diagram. The arrows indicate the transition between the different electronic states. Radiative processes are shown , absorption is represented by the blue arrow , emission is represented by the bright green arrow and phosphorescence is represented by the orange arrow. The non-radiative processes, such as internal conversion, intersystem crossing and vibrational relaxation are shown in red, flat green and maroon respectively.

The absorbance (A) is determined as a ratio of the intensity of light before (Io) and after (I) it passes through an optical cell according to (Eq 1).

$$A = \log \frac{I_o}{I} \qquad (1)$$

based on the absorbance value, the concentration of the protein sample can be determined using Beers Lambert Law (Eq. 2).

$$A = \varepsilon bc \qquad (2)$$

where ε is the extinction coefficient in $cm^{-1}M^{-1}$, b is the pathway in cm and c is the concentration in mol L^{-1}. The values of extinction coefficients used in this study are summarized in Table 2.1.

Table 2.1: Extinction coefficient values used in this study

	λ max (nm)	Extinction coefficient ($cm^{-1}M^{-1}$)	Source
DREAM WT	280	19 000	(Azam & Miksovska, 2019)
DREAM-NCS 1	280	19 000	(Azam & Miksovska, 2019)
1,8-ANS	350	5000	(Stryer, 1965)
Kv 4.3 Site 1	493	80 000	(Azam & Miksovska, 2019)
Kv 4.3 Site 2	493	75 000	(Azam & Miksovska, 2019)

2.4 Steady state emission

The emission spectrum is the measure of the light intensity emitted by a sample as a function of wavelength, after the sample has been excited at a specific wavelength (Jameson, 2014; Lakowicz, 2006). The Trp residue is a commonly used intrinsic probe in proteins as its emission properties can be used to monitor protein tertiary structure changes due to its sensibility to the surrounding environment, (Jameson, 2014)

The DREAM protein has a unique Trp residue in position 169 located in a hydrophobic cavity (Lusin et al., 2008) , which was used to monitored changes in the protein tertiary structure upon Ca^{2+} association to the protein. The Trp emission spectra were recorded

using PC1 fluorimeter. The samples were excited with a 280 nm output from the Xe lamp and emission was collected in 90-degree orientation from 300 nm to 470 nm. The samples for emission measurements contained 10-µM protein solubilized in 20 mM Tris buffer pH 7.4. The sample was placed in a 0.1x1.0 cm or 0.2 x 1.0 cm quartz cuvette. The apo, Mg^{2+}, Ca^{2+} and $Mg^{2+}Ca^{2+}$ bound protein was prepared by adding 5 mM EDTA,5 mM EGTA, 1 mM $MgCl_2$ and/or 1 mM $CaCl_2$ to the protein samples.

2.5 Fluorescence lifetime

Fluorescence lifetime of fluorophore (τ) is the measure of how much time the molecule spends in the excited state, corresponding to the time between absorption and emission (Jameson, 2014), and is commonly expressed using Eq. 3, where τ is the lifetime in ns , k_{rad} is the rate constant for radiative processes and k_{nonrad} is the rate constant for non-radiative processes.

$$\tau = \frac{1}{krad+knonrad} \quad (3)$$

The information of the lifetime of intrinsic or extrinsic fluorescence probes in protein provide additional information and structural and dynamic properties in protein and are important for interpreting other parameters such as lifetime and anisotropy (Jameson, 2014). Fluorescence lifetime can be measured using the time domain or the frequency domain approach (Jameson, 2014). In the time domain approach the sample is excites with a short laser pulse and the change in intensity is measured as a function of time (Jameson, 2014). On the other hand, in the frequency domain approach, the sample is excited using a continuous light source modulated at different high frequencies (20 MHz to 200 MHz))

in a sinusoidal manner, as a result of the excitation the sample, the emitted light shown a frequency phase shift and amplitude modulation with respect to the excitation source modulated emission light (Jameson, 2014; Lakowicz, 2006). The lifetime can be determined by analyzing the experimental data using several models such as sum of multiple exponential decay, Gaussian distribution, Lorents distribution etc. (Jameson, 2014) . The lifetime data presented in this study were measured in the frequency domain using Chrono FM fluorometer (ISS, Chapagain Illinois)

The samples for Trp fluorescence lifetime measurements contained 20 μM protein in 20 mM Tris buffer pH 7.4. The apo, Mg^{2+}, Ca^{2+} and $Mg^{2+}Ca^{2+}$ bound proteins were prepared by adding 5 mM EDTA, 5 mM EGTA, 1 mM $MgCl_2$ and/or 1 mM $CaCl_2$ into proteins samples. The compound 2.5-diphenyl-oxazole (PPO) with the lifetime of 1.4 ns was used as a reference. The sample was excited with 280 nm laser diode and the emission intensity was collected using a 300 nm long pass filter (Andover). The plots of phase modulation and phase shift as a function of modulation frequency were fitted using a three exponential decays model. The quality of the fit was judged by a χ^2 value and residual.

The samples for measuring emission lifetime of DREAM in the presence of 1,8-ANS contained 20 μM protein in 20 mM Tris buffer pH 7.4 and 20 μM 1,8-ANS. The apo, Mg^{2+}, Ca^{2+} and $Mg^{2+}Ca^{2+}$ bound proteins were prepared by adding 5 mM EDTA, 5 mM EGTA, 1 mM $MgCl_2$ and/or 1 mM $CaCl_2$ into proteins samples. The samples were placed in a 0.1x1.0 cm or 0.2 x 1.0 cm quartz cuvette and the output of 305 nm diode was used for the excitation. The emission intensity was collected using a 400 nm long pass filter (Andover Corp). The plots of phase modulation and phase shift as a function of modulation frequency

were fitted using a three exponential decays model. The quality of the fit was judged by a χ^2 value and residual.

2.6 Anisotropy

Anisotropy measurements allow to determine rotational mobility of a fluorophore by monitoring the ratio of the emitted light using different orientation of polarizers placed in the excitation and emission path according to Eq 4. (Jameson, 2014).

$$A = \frac{I_{II} - I_{\perp}}{I_{II} + 2I_{\perp}} \qquad (4)$$

where A represents anisotropy and I_{II} and $I_{\perp}$ represent the parallel and perpendicular orientation of the polarizers. In general, the excitation light passes through a polarizer placed in the excitation path and only fluorophore molecules that have a transition dipole

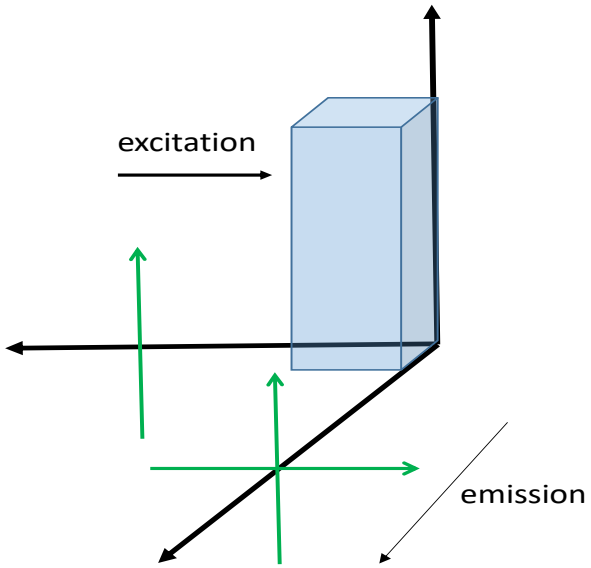

Fig. 2.2: Position of the polarizers for the steady-state anisotropy measurements. The Direction of the propagation of the excitation light and collected emitted light are shown as thin black arrows, the orientation of the polarizer placed in the excitation and emission path are shown in green. (Adapted from Jameson 2004).

moment aligned with the electric field of the excitation light are excited. The polarization of the emitted light corresponds to the orientation of the transient dipole moment of the excited molecule at the time of light emission (Lakowicz, 2006). For small molecules that freely rotate in the solution, the emitted light is depolarized, whereas light emitted by molecules or molecules trapped in a membrane or a solid like environment emit light polarized in the orientation analogous to the polarization of the excitation light. (Jameson, 2014) A second polarizer placed in the path of the emitted light is in a parallel or perpendicular orientation with respect to the polarizer placed in the excitation path and the emission intensity is collected. As anisotropy values are usually proportional to the size of the fluorescent molecule, anisotropy represent a convenient approach to characterized binding of small fluorescent molecules to proteins. By measuring anisotropy as a function of an increasing concentration of the protein, the binding isotherm for fluorophore association to the protein can be constructed and the equilibrium association or dissociation constants can be determined by analyzing the experimental data using an appropriate model.

Here we used the anisotropy approach to measure the dissociation constant for binding of fluorescent labeled peptides that mimic DREAM binding sites in the T1 domain of potassium voltage channels, so called site 1 and site 2. The site 1 corresponds to the residues 2 to 22 of the T1 domain (FITC-AAGVAAWLPFARAAAIGWMPV)) and the site 2 corresponds to the residues 70 to 90 of the T1 domain (FITC-LLGSTEKEFFFNEDTKEYFFD). The peptides were labeled by a fluorescent probe fluorescein isothiocyanate (FITC) (Scheme 2.1) covalently attached the peptide N-terminal.

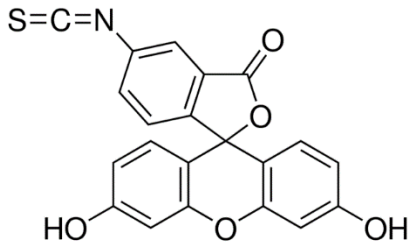

Fig. 2.3: Structure of FITC

Peptides were solubilized in 20 mM Tris buffer pH 7.8 and anisotropy was measured using 390 nm excitation light. The emission was collected through a long pass 500 nm filter placed in the emission light pathway. Subsequently small aliquots of DREAM WT or DREAM-NCS1 protein were added and anisotropy values were recorded. Each value of anisotropy corresponds to an average value determined for 10 measurements. The values of the anisotropy change were plotted as a function of protein concentration and the titration curves were analyzed using quadratic equation (Eq. 5) and assuming a single binding site for each peptide.

$$\Delta A = \frac{(K_d + [P_t] + [L_t]) - \sqrt{(K_d + [P_t] + [L_t])^2 - 4[P_t][L_t]}}{2c} \qquad (5)$$

where ΔA is the change in anisotropy, K_d is the equilibrium dissociation constant, P_t is the total concentration of protein in the sample, L_t is the total ligand concentration of 0.5 µM, and c is the proportionality constant.

2.7 Circular Dichroism

Circular dichroism (CD) is a widely used technique to study protein secondary structure as well as protein stability (Greenfield, 2007). In CD measurements, difference in the absorbance of the right and left circularly polarized light in the far ultraviolet (UV) and near UV spectrum is determined as chiral chromophore have a different extinction coefficient for the left and right circularly polarized light. (Greenfield, 2007). The CD spectra of protein in the far UV (190 nm to 250 nm) provides information of the secondary structure of proteins major secondary structure elements, α-helices, β-sheets and random coil, have a distinct CD spectrum as shown in Fig. 2.3.

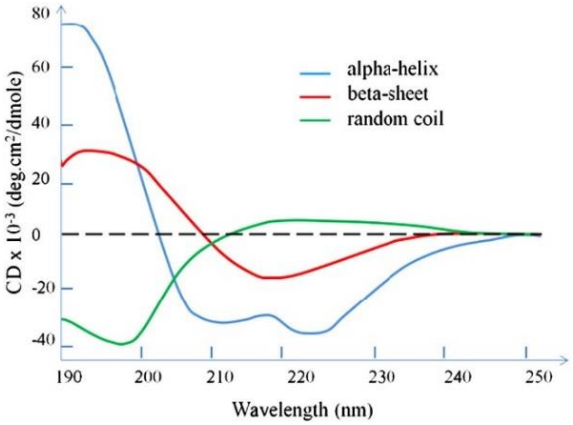

Fig. 2.4: Typical CD spectra, showing the three major secondary structures of proteins, α-helix, β-sheet and random coil with distinctive peak at specific wavelengths. Adapted from Wei *et al.* (Wei, Thyparambil, & Latour, 2014)

For instance, α helical structures show a strong positive peak at 192 nm and two negative peaks at 208 and 222 nm. In the case of β sheets, a negative peak at 218 nm and a positive peak at 196 nm are observed whereas random coils show only a very week CD signal (Greenfield, 2007). The monitoring of CD spectra in the near UV region are less common,

however these data can provide information about structural changes in the environment of aromatic residues Phe, Tyr and Trp.

The samples for CD measurement contained 20 µM protein in 20 mM Tris buffer pH 7.4 placed in a 0.1 mm x1 cm quartz cuvette. The apo, Mg^{2+}, Ca^{2+} and $Mg^{2+}Ca^{2+}$ bound DREAM was prepared by adding 5 mM EDTA,5 mM EGTA, 1 mM $MgCl_2$ and/or 1 mM $CaCl_2$ to the protein samples. The data were collected from 190 to 260 nm using a J-810 Jasco CD spectrometer.

2.8 Isothermal Calorimetry

Isothermal calorimetry is a widely used analytical technique, which provides thermodynamic parameters such as K_{eq}, ΔG, ΔH and ΔS using Eq (6) and (7)

$$\Delta G = -RTlnK \qquad (6)$$

$$\Delta G = \Delta H - T\Delta S \qquad (7)$$

It determines the heat in a reaction process proportional to the molar enthalpy change associated with the process and the amount of complex formed.

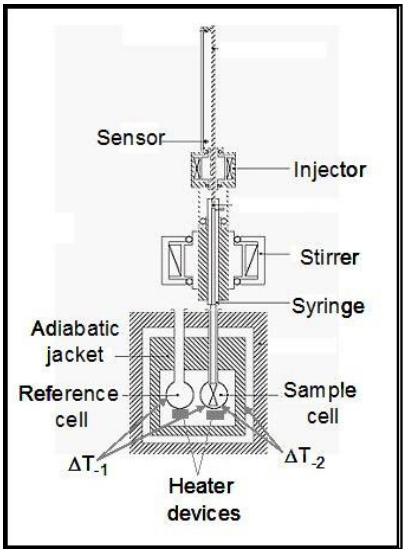

Fig. 2.5: ITC instrumentation. Adapted from (Martinez et al., 2013)

The ITC experiments were performed employing a VP-ITC MicroCalorimeter (MicroCal LLC, Northampton MA). The ITC instrument contains an adiabatic jacket with a reference and a sample cell, where the titration occurs. The sensor measures the amount of heat needed to keep the sample and reference cell temperature constant with every addition of ligand, providing a heat signal as a function of time. The heat signal is integrated and plotted as a function of molar ratios of the ligand and protein. The ITC data are then analyzed using fitting models in Origin 7 software to calculate thermodynamic parameters including number of binding sites (n), equilibrium association constant (Ka), reaction enthanlpy change (ΔH) and reaction entropy change (ΔS) (MicroCal, LLC, Northampton, USA). In the experiments presented in Chapter 3, the experimental data were fitted to one sequential binding site model.

3. INTERACTIONS OF DREAM WITH Zn^{2+} ION.

3.1 Introduction

Zinc is a key element in neuronal growth and activity and it is necessary for the normal development and functioning of the brain (Plum, Rink, & Haase, 2010; Vallee & Falchuk, 1993). It has been found to interact with more than 50 different types of protein that require Zn^{2+} to function (Vallee & Falchuk, 1993). It can be found intracellularly in concentrations around the 100 pM and the free Zn^{2+} varies in nm-pM range (Plum et al., 2010). The regulation of the physiological concentration of Zn^{2+} is crucial for the normal functioning of the organism (Plum et al., 2010).

Zinc deficiency produces growth retardation and immune system dysfunctions (Plum et al., 2010). Furthermore, neurologically there are several effects such as decreased nerve conduction, neuropsychiatric disorders and mental lethargy (Plum et al., 2010).Whereas a Zn^{2+} excess also affects the body by altering the lymphocyte function, producing gastrointestinal issues and copper deficiency (Plum et al., 2010). In the brain, Zn^{2+} excess causes lethargy and focal neuronal deficits (Plum et al., 2010). Recently, Permyakov *et al*. have shown that Zn^{2+} binds to the member of neuronal calcium sensor family, recoverin with a K_d of 7.0 μM (Permyakov, S. E. et al., 2003). Therefore, considering the role of Zn^{2+} in neuropathology and the high homology between recoverin and DREAM, as shown in Figure 3.1, I suggest that DREAM may serve as a molecular target for Zn^{2+}. To test Zn^{2+} interactions with DREAM I characterized DREAM emission properties in the presence of DREAM as well as circular dichroism and isothermal titration calorimetry studies.

Fig. 3.1: Sequence similarity among recoverin (PDB entry 1JSA) and DREAM (PDB entry 2JUL), identical residues in green, similar residues in pink, sequence mismatch in blue and insertion/deletion in brown. Obtained from RCSB PDB Protein Comparison Tool. Smith-Waterman sequence alignment (Smith & Waterman, 1981)

3.2 Steady state fluorescence emission

The Trp intrinsic fluorescence emission for the DREAM WT exhibits specific transitions upon divalent metals addition along with a typical λ_{max} at 330 nm. For DREAM WT, the intensity decreases upon Ca^{2+} and $Ca^{2+}Mg^{2+}$ addition, whereas for addition of Mg^{2+} no transition is observed with respect to the apo form. Emission spectra for Trp 169 were detected upon Zn^{2+} addition to DREAM in the presence and absence of divalent metals, to monitor Zn^{2+} binding to DREAM and its impact on Trp 169 surrounding. For the apo, Ca^{2+}, Mg^{2+} and $Ca^{2+}Mg^{2+}$ bound forms the Zn^{2+} addition resulted in an increase in the emission at 330 nm, suggesting Zn^{2+} binds to the protein and triggers changes in the Trp environment.

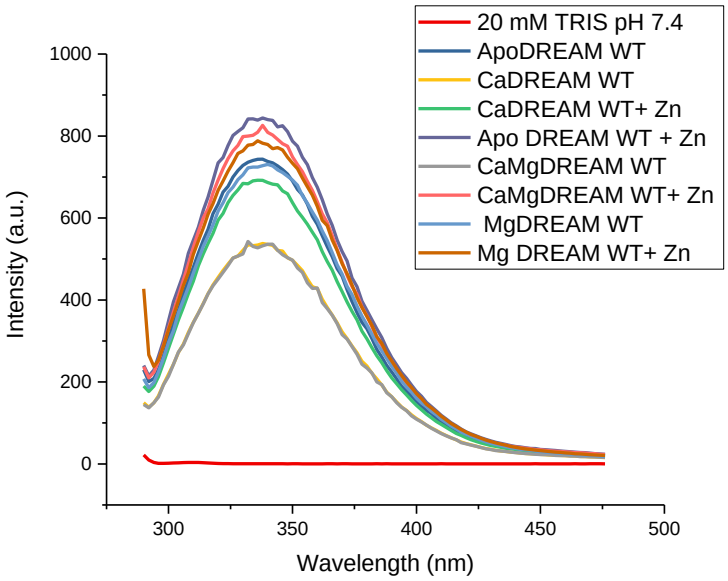

Fig. 3.2: Steady-state fluorescence emission of Trp for DREAM-WT upon 500 µM Zn^{2+} addition in the presence and absence of Ca^{2+} and/or Mg^{2+}.

Furthermore, titration curves for Zn^{2+} binding to DREAM WT were obtained by adding increasing concentration of Zn^{2+} to DREAM samples and the Trp emission intensity was monitored in the presence and absence of Ca^{2+} shown in Fig.ure 3.3.

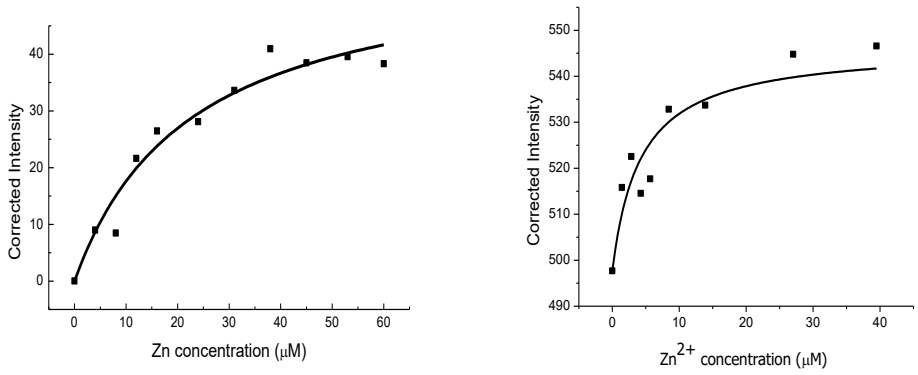

Fig. 3.3: Trp fluorescence emission for the Zn^{2+} association to Ca^{2+} (right) and apo (left) DREAM WT

The equilibrium dissociation constants were determined and are shown in Table 3.1. Dissociation constant for Zn2+ binding to the apo form of the protein is around 3 times lower than the one for the Ca^{2+}bound form , suggesting a stronger affinity of Zn^{2+} for DREAM WT in the absence of Ca^{2+}.

	K_d (μM)
Apo DREAMWT	4.3±0.9
Ca^{2+} DREAMWT	14.0±3.1

Table 3.1: Dissociation constant for Zn^{2+} association to DREAMWT in the presence and absence of Ca^{2+}.

3.3 CD measurements

The secondary structure changes upon Zn^{2+} addition to the protein were measured using circular dichroism for DREAM WT in the absence and presence of divalent metals shown in Fig.ure 3.6

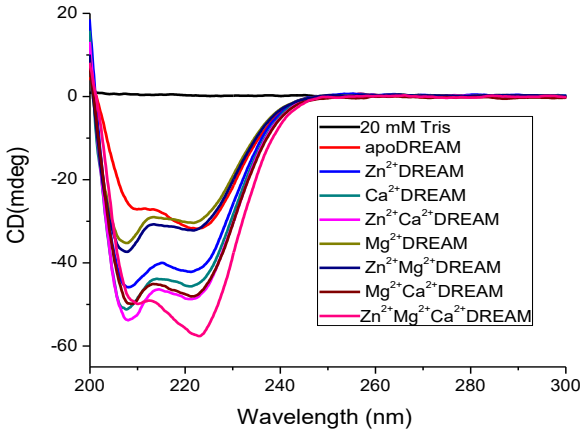

Fig. 3.4: Secondary structure characterization of DREAM WT upon Zn^{2+} addition in the absence and presence of Ca^{2+}, Mg^{2+} and $Ca^{2+}Mg^{2+}$.

A decrease in CD signal was observe upon Zn^{2+} in all the cases , for the apo form a more pronounced decrease in the CD signal was observed when compared to the Ca^{2+} , Mg^{2+} and $Ca^{2+}Mg^{2+}$ forms. Suggesting the Zn^{2+} binding to apo DREAM leads to the significant increase in the protein secondary structure and possibly to the stabilization of the protein structure. In decrease in the CD signal in the presence of Mg^{2+} and Ca2+ was less pronounced, suggesting that the presence of Mg^{2+} and Ca^{2+} in the EF-hands modulates Zn2+ impact on the protein secondary structure.

3.4 Impact of Zn^{2+} on DREAM interactions with hydrophobic probe, 1,8-ANS

The fluorescence emission of 1,8 ANS-DREAM complex in the presence and/or absence of Ca^{2+}, Mg^{2+} was monitored in order to determine impact of Zn2+ binding on the accessibility of hydrophobic surfaces on the protein surface . The emission spectra for DREAM in the absence/ presence of divalent ions are shown in Figure 3.4 .

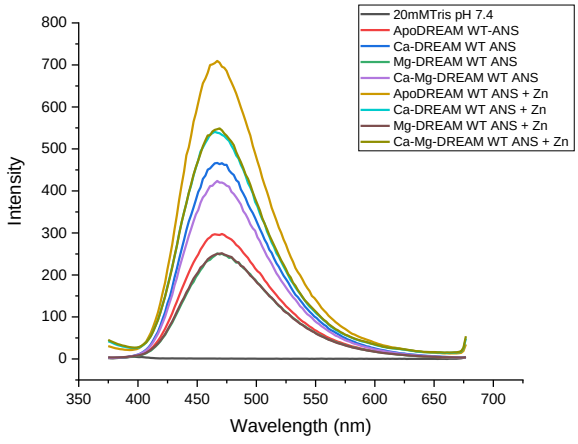

Fig. 3.5: Emission spectra of 1,8 ANS-DREAM WT complex in the presence and/or absence of Ca^{2+}, Mg^{2+} and Zn^{2+}.

For the 1,8 ANS-DREAMWT apo, Ca^{2+} , and $Ca^{2+}Mg^{2+}$ bound forms the Zn^{2+} addition resulted in an increase in the 1,8-ANS emission intensity. The largest increase in intensity was observed for the apo form and interestingly for the Mg^{2+} bound form of DREAM W, the Zn^{2+} triggered changes in the emission intensity were negligible that is consistent with the CD data. Furthermore, the equilibrium dissociation constant for 1,8 ANS binding to DREAM in the presence of Zn^{2+} was determined by monitoring the increase in the emission intensity upon Zn^{2+} titration into 1,8 ANS-DREAMWT complex in the presence and absence of Ca^{2+} . The corresponding titration curves areas shown in Figure 3.6.

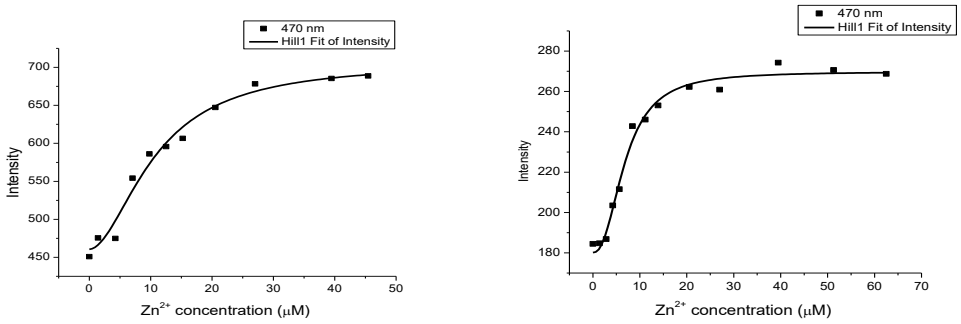

Fig. 3.6: Zn^{2+} association to Ca^{2+} and Apo DREAM WT in the presence of 1,8 ANS

The Kd values were obtained by fitting the data using the Hill equation (Eq. 4.1) and are shown in Table 3.2. Slightly smaller K_d value was determined for apoDREAM compared to the Ca^{2+} bound protein, in agreement with the Trp emission data.

	K_d (μM)
Apo DREAMWT	6.9 ± 0.6
Ca^{2+}DREAMWT	10.76± 1.46

Table 3.2: Dissociation constant for 1,8 ANS - DREAMWT association with Zn^{2+} in the presence and absence of Ca^{2+}.

In addition, the impact of Zn^{2+} on the fluorescence lifetimes of 1,8-ANS: DREAM complex in the presence and absence of Ca^{2+} was probed using frequency modulation approach and the date are presented in Fig. 3.7 . The lifetime values were obtained from a fit of experimental data using a three exponential decay model and the fitting parameters are summarized in Table 3.3. The lifetime for unbound 1,8-ANS was fixed to 0.27 ns (Gonzalez & Miksovska, 2014). Upon Zn^{2+} addition, τ_1 decreased from 5.9 ns to approximately 3.0 ns for both apo and Ca^{2+}bound protein, while Zn^{2+} association does not impact the longer lifetime, τ_2. These results suggest that the 1,8-ANS-binding site with the shorter lifetime, τ_1, is more sensitive to the structural changes triggered Zn^{2+} binding whereas the emission properties of 1,8-ANS bound to the second site are only slightly affected by the Zn^{2+} association.

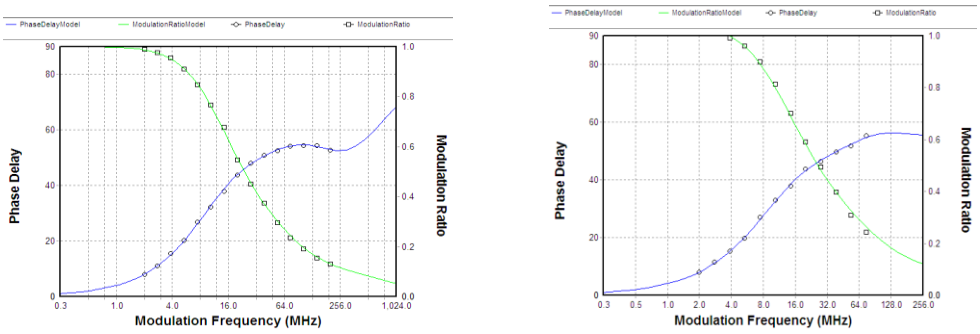

Fig. 3.7: Frequency domain intensity decay for Zn^{2+} addition to Ca^{2+} bound 1,8-ANS-DREAMWT (left) and 1,8 ANS- apo DREAM-WT (right). The solid lines correspond to the fit of the experimental data using a sum of three exponential decay model.

Table 3.3: 1,8 ANS lifetime for apo and Ca-DREAM WT in the presence of Zn^{2+}fitted to three exponential decays with a fixed lifetime for 1,8 ANS of 0.27 ns. The lifetime values for 1,8 ANS bound to DREAM in the absence of Zn^{2+} were previously determined by Gonzalez (Gonzalez & Miksovska, 2014)

	τ_1 (ns)	τ_2 (ns)	α_1	α_2	χ^2
1,8 ANS Apo DREAM WT	5.9± 0.1	16.2 ± 0.7	0.13	0.23	1.16
1,8 ANS Ca^{2+}DREAM WT	5.9± 0.2	17.6 ± 0.5	0.18	0.42	1.13
1,8 ANS-Apo DREAMWT+ Zn^{2+}	2.89 ± 0.2	14.4 ± 0.2	0.07	0.06	9.45
1,8 ANS-Ca^{2+}DREAMWT+Zn^{2+}	3.13 ± 0.09	14.1 ± 0.1	0.05	0.05	4.05

3.5 ITC studies

Isothermal calorimetry studies were performed to determine the dissociation constant and thermodynamic parameters for Zn^{2+} binding to apo DREAM. The binding isotherm is shown in Fig. 3.8. The data were analyzed using one binding site model. The Zn^{2+} binding to the protein is exothermic, with the reaction enthalpy change of -5.1 kcal mol^{-1} (Table 3.4) and the equilibrium dissociation constant was determined to be 3±1 μM. This value of 3±1 μM is similar to the K_d value obtained from monitoring changes in Trp 169 emission in apo DREAM, K_d = 4.3±0.9 μM and 1,8-ANS:apoDREAM emission, K_d = 6.9 ± 0.6 μM.

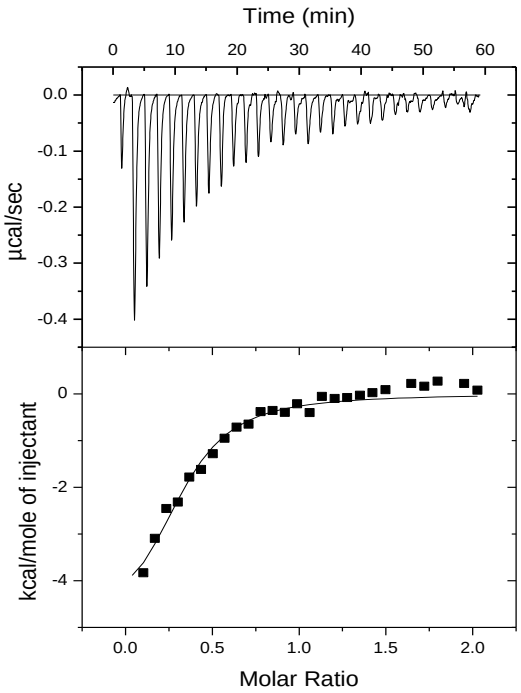

Fig. 3.8: ITC Isotherms for Zn^{2+} association to DREAM in the absence of Ca^{2+}, the upper panel refers to thermal power as function of time, and the lower panel represent the integrated reaction heat ΔH in kcal/mol.

	K_D (µM)	ΔH (kcal/mol)	TΔS (kcal/mol)
Zn^{2+}apo DREAM WT	2.6± 1.0	- 5.1	23.7

Table 3.4: Equilibrium Dissociation constant of Zn^{2+} binding to DREAM in the absence of Ca^{2+}Using one model sequential binding fitting.

3.6 Discussion

The fluorescence and CD results presented in the chapter for Zn^{2+} interactions with DREAM suggest that Zn^{2+} binds to DREAM with relatively high affinity, $K_d \sim 5$ µM. The increase in the emission spectra for the Trp residue indicates that Zn^{2+} association impact the tertiary structure of the protein. The dissociation constant obtained for Zn^{2+} binding to apo and Ca^{2+} DREAM of 5 µM and 14 µM, respectively, is similar to the value reported for recoverin, Kd = 7 µM (Permyakov, S. E. et al., 2003). The dissociation constant obtained for Zn^{2+} binding to DREAM in the absence of Ca^{2+} through fluoresce emission of 4µM, is very close to the K_d = 3 µM obtained through isothermal calorimetry measurements, suggesting a higher affinity of Zn^{2+} to DREAM in the absence of the physiological ligand. In addition, the decrease in the CD signal suggest a stabilizing effect on the protein structure similar to the one occurring upon Ca^{2+} addition. Furthermore, the addition of Zn^{2+} to 1,8 ANS –DREAM complex resulted in an increase in the fluorescence intensity, suggesting a higher exposure of the hydrophobic surfaces due to the Zn^{2+} binding. The emission data is in agreement with the 1,8 ANS lifetime values, which demonstrate a lower τ_1 upon Zn^{2+} addition, suggesting that 1,8 ANS binding site 1 is more sensitive to the Zn^{2+} conformational changes. Overall, the data obtained confirm that Zn^{2+} binds to DREAM in apo and Ca^{2+} bound form, and association of Zn+ to the protein triggers changes in protein. Maret *et al* studied zinc-protein interactions and reported that Zn^{2+} is usually coordinated in proteins by four ligands with the side chain of Cys, His, Glu, or Asp being the most common ligands (Maret & Li, 2009). The inspection of the monomeric

structure of the calcium bound protein (PDB entry 2JUL, Lusin et al, 2008) did not reveal a possible binding site on the DREAM monomer. However, it is likely that the Zn^{2+} association to the protein requires the presence of the apo protein tetramer or Ca^{2+} bound protein dimer and thus additional studies are necessary to identify residues that participate in Zn^{2+} coordination.

4. MOLECULAR MECHANISM OF DREAM DIMERIZATION

4.1 Introduction

Unlike traditional EF hand sensors, such as calmodulin and troponin C that remind in the monomeric form in the absence and presence of Ca^{2+}, Ca^{2+} association to other CBPs triggeres a structural transition that facilittes protein oligomeriztion. For example, proteins belonging to S100 calcium binding protein subfamily are known to undergo dimerization upon Ca^{2+} binding to the EF hands. Some members of the neuronal calcium sensor family also undergo Ca^{2+} triggered dimerization such as recoverin, GCAP 1-5 and VILIP-1(Ames, 2018) (James 2018[JM3]). The available structures of dimeric form of individual proteins suggest, that each protein adopt a unique dimeric structure, as shown in Fig.ure 4.1, likely due to a distinc physiological role of each proteins (James, 2018). For example, the dimeric structure of Ca^{2+} bound VILIP-1 shows that the binding interface is formed through contacts beween α-helices located in EF-hand 4 of the C- terminal domain (Li, Pan, Braunewell, & Ames, 2011) (Li et al., 2011[JM4]), whereas in recoverin, the exiting α-helix from the EF-hand 4 interacts with hydrophobic residues in a cavity located between EF-hand 1 and EF-hand 2 (Myers et al., 2013) (Myers et al., 2013[JM5])

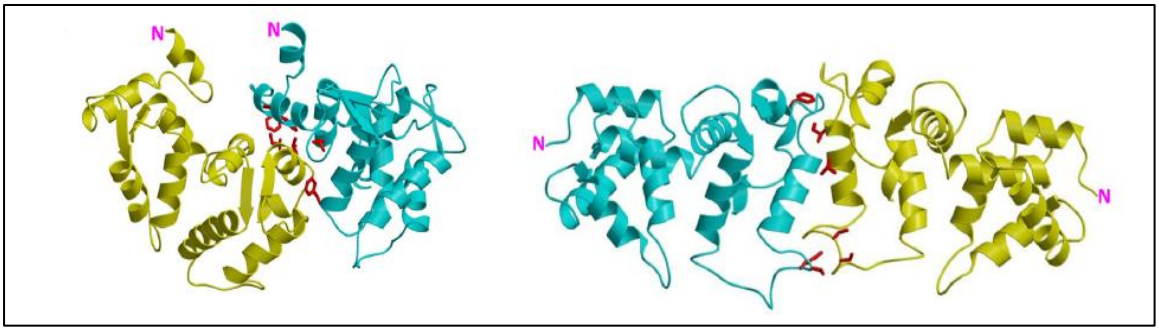

Fig. 4.1: The structure of the dimeric form of recovering (left) and VILIP-1 (right) in Ca^{2+} bound form. Individual monomers are colored in yellow and blue and side chains of residues in the binding interfaces are shown in red. Adapted from Ames 2018 (Ames, 2018)

Based on the NMR structure of Ca^{2+} bound DREAM monomer, Lusin et al. suggested that DREAM forms a dimeric structure with the head to tail orientation of the C- and N-terminal domain (Lusin et al, 2018). The dimeric form was proposed to be stabilized by hydrohobic interactions between Leu residues in the N- terminal domain (Leu 155 and Leu 159) of one monomer and Leu 251 in the C- terminal domain of the second monomer. Albeit replacement of Leu residues by Ala did not abolished the formation of the dimers, but the equilibrium constant for the protein dimerization decreased (Lusin et al, 2018). The DREAM dimeric structure is destabilized at an increased concentration on sodium chloride as observed in the homo Förster resonance energy transfer measurement , suggesting that ionic interactions also contribute to the formation of DREAM dimeric form (unpublished results from Dr. Miksovska group).

In order to better understand the mechanism of Ca^{2+} triggered protein dimerization and the mechanism of signal transduction in DREAM, we prepared a DREAM construct with the aim to abolish protein dimerization. Based on the previously published model structure of DREAM (Lusin et al, 2018), a protein docking and molecular dynamic simulation of the

DREAM dimer structure, Fig. 4.3, (Miksovska laboratory, unpublished results) and the fact that other member of neuronal calcium sensor family, NCS1, does not form a dimer[JM6] (Pandalaneni et al., 2015), I proposed to construct a chimeric variant of a protein with Leu residues in position 155 and 158 replaced by residues Thr and Leu, that are found in NCS-1 respectively. In addition, since the simulated structure of DREAM dimer shows an interactions between Arg residues(Arg 200 and Arg 208) in the long loop conecting EF-hand 3 and EF-hand 4, the residues in the loop were replaced by residues found in the loop in NCS-1. I label this chimeric form of the protein DREAM-NCS-1. The alignment of the sequence of DREAM-NCS-1 and the sequence of DREAM WT in Fig. 4.2. The properties of DREAM-NCS-1 variant were characterized using fluorescence and CD spectroscopy and the interactions with the peptides mimicking the DREAM binding sites in T1 domain of potassium voltage channels were determined.

MELELSTVRHQPEGLDQLQAQTKFTKKELQSLYRGFKNECPTGLVDEDTFKLIYSQFFPQGDATTYAHFLFNAFDAD
MELELSTVRHQPEGLDQLQAQTKFTKKELQSLYRGFKNECPTGLVDEDTFKLIYSQFFPQGDATTYAHFLFNAFDAD

GNGAIHFEDFVVGLSILLRGTVHEKLKWAFNLYDINKDGCITKEEMLAIMKSIYDMMGRHTYPILREDAPLEHVERF
GNGAIHFEDFVVGLSITSRGTVHEKLKWAFNLYDINKDGCITKEEMLAIMKSIYDMMGNTVELPEEEDAPLEHVERF

FQKMDRNQDGVVTIDEFLETCQKDENIMNSMQLFENVIYLEHHHHHH
FQKMDRNQDGVVTIDEFLETCQKDENIMNSMQLFENVIYLEHHHHHH

Fig. 4.2: Sequence of mouse DREAM WT (red) with a start methionine residue (green) and a C-terminus His-tag (blue) connected by tripeptide linker (green). The DREAM-NCS (black) has identical sequence to the DREAM WT except residues L158, Leu159 replaced by Thr and Ser and the loop between EF-hand 3 and 4 (shown in yellow) replaced by the amino acid sequence found in human NCS-1 (shown in bold red).

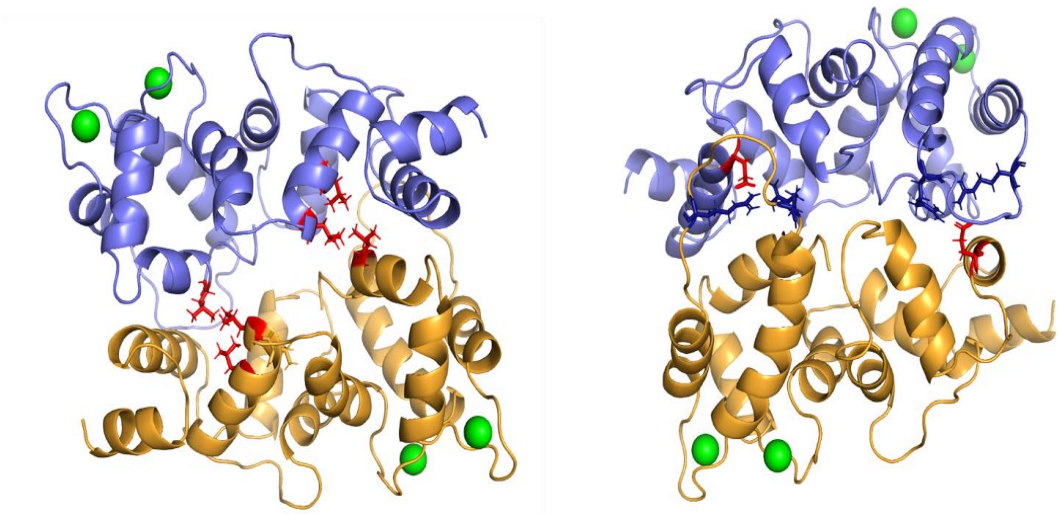

Fig. 4.3: Model structure of DREAM dimer based on the NMR structure of DREAM monomer (PDB entry 2JUL). Left panel shows hydrophobic interactions between Leu 155, 159 and 251 and right panel show a salt bridge between Arg 200, Arg 207 (in blue) and Glu 103 (in red).

4.2 Steady state fluorescence emission

Trp 169 fluorescence emission spectrum of DREAM WT presents a characteristic λ_{max} at 330 nm, Fig. 4.4. The emission intensity decreases upon Ca^{2+} and $Ca^{2+}Mg^{2+}$ addition to the apo protein sample, whereas upon addition of Mg^{2+}, no changes are observed with respect to apoDREAM WT. Interestingly, when analyzing the Trp steady state emission of the DREAM-NCS1 variant, the spectrum of the apoform exhibits a red shift with respect to DREAM WT, with a λ_{max} at 337 nm. Furthermore, , the emission intensity increases upon Ca^{2+} and $Ca^{2+}Mg^{2+}$ addition , while Mg^{2+} binding to the apoprotein does not modulate the emission intensity as shown in Fig. 4.4. The increase in the Trp 169 emission observed for Ca^{2+}DREAM-NCS-1 is distinct from the DREAM WT, which exhibits an opposite trend, decrease in the emission internist in the presence of Ca^{2+}.

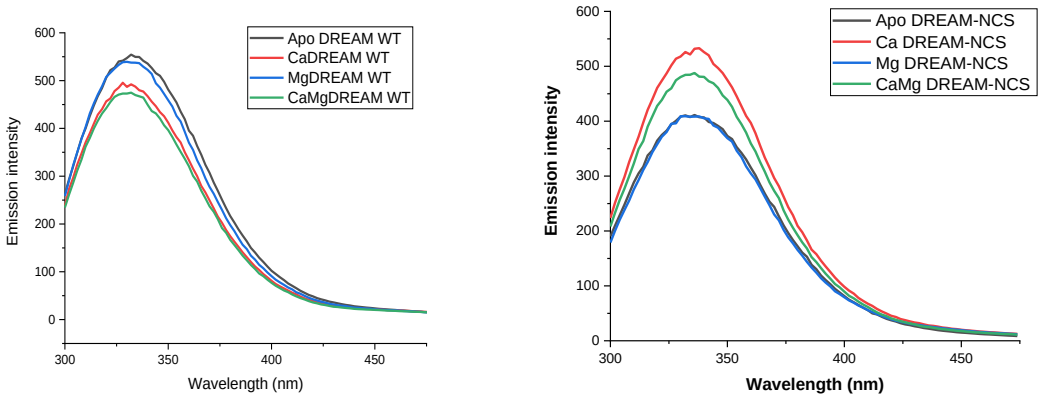

Fig. 4.4: Steady-state fluorescence emission of Trp for DREAM-WT (left) and DREAM-NCS1 (right) in the presence and absence of Ca^{2+} and/or Mg^{2+}.

4.3 CD spectra

The changes in the secondary structure were monitored by performing CD measurements for both DREAM WT and DREAM-NCS 1 in the presence and absence of divalent metals. For DREAM WT and DREAM-NCS 1 a decrease in the CD signal is observed upon addition of divalent metals, similar to other NCS where Ca^{2+} binding leads to the increase in the α-helical contain of the protein Azam at al, 2019 (Azam & Miksovska, 2019)[JM7]. These results together with the emission data indicate that Ca^{2+} binds to the chimeric version of the protein. In addition, the substitution of Leu residues and the modification of the loop connecting the EF-hand 3 and EF-hand 4 does not destabilizes the protein secondary structure and protein fold.

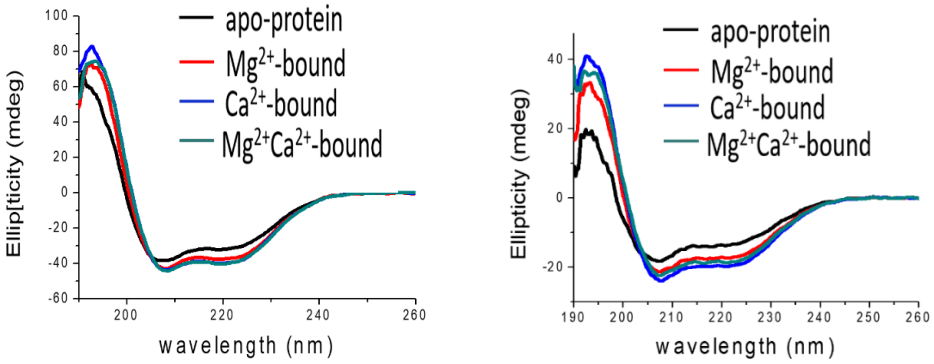

Fig. 4.5: Circular dichroism spectra for DREAM WT (left) , and DREAM-NCS1 (right) in the presence and absence of Ca^{2+} and/or Mg^{2+}.

4.4 Ca^{2+} triggered exposure of hydrophobic cavities

1,8-ANS is a small hydrophobic molecule that is very weakly fluorescent in aqueous solution but its fluorescent quantum yield increases significantly upon binding to hydrophobic cavities on a protein surface (Gasymov & Glasgow, 2007) . Two binding sites with a high affinity for 1,8-ANS were identified for DREAM WT in the C-terminal domain and the analysis of the emission data indicates that 1,8-ANS binds to DREAM WT in Ca^{2+} dependent manner. (Gonzalez & Miksovska, 2014) The emission spectra of 1,8-ANS bound to DREAM-NCS 1 in the apo form and in the presence of Ca^{2+} and/or Mg^{2+} are shown in Fig. 4.6. The results show a transition towards increase emission intensity of 1,8-ANS upon binding of Ca^{2+}as well as in the presence of Mg^{2+}. The λ_{max} for apo DREAM is around the 471 nm, while the metal bound protein exhibits a red to a λmax of 491 nm shift with respect to apo DREAM.

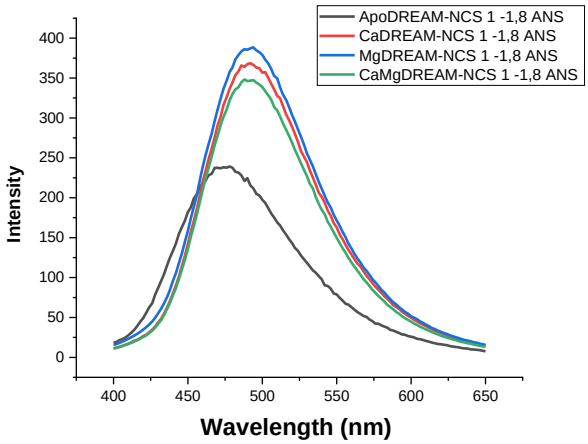

Fig. 4.6: 1,8 ANS-DREAM-NCS 1 emission spectra upon Ca^{2+} , Mg^{2+} and $Ca^{2+}Mg^{2+}$ addition.

In order to gain more information about 1,8-ANS interactions with DREAM-NCS-1, the equilibrium dissociation constant for 1,8- ANS binding to DREAM were determined by titrating apo DREAM-NCS 1 and Ca^{2+} DREAM-NCS-1 with 1,8-ANS. The titration curves were constructed by plotting the increase in the emission intensity for 1,8-ANS additions to DREAM-NCS-1 as shown in Fig. 4.7.

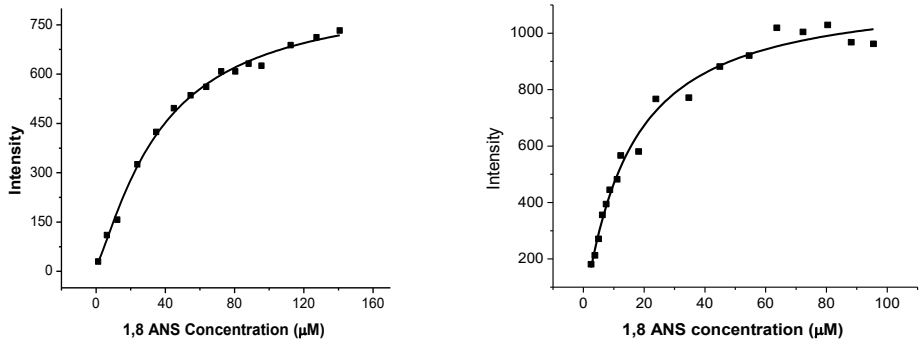

Fig. 4.7: Titration curves for 1,8-ANS binding to apoDREAM-NCS 1 (left) and Ca^{2+}DREAM-NCS 1 (right).

Affinity constants for 1,8-ANS binding to apoDREAM-NCS-1 and Ca^{2+} bound DREAM were determined by analyzing the titration curves using Hill equation (Eq. 4.1):

$$F = B_{max} \frac{[1,8-ANS]^n}{[1,8-ANS]^n + K_D} \quad (4.1)$$

where F is the observed emission intensity, n is the Hill coefficient, K_D is the equilibrium dissociation constant and B_{max} is the proportionality constant. The fitting parameters are summarized in Table 4.1 together with the data obtained for 1,8-ANS binding to DREAM WT. Interestingly, the affinity of 1,8-ANS for DREAM-NCS-1 increased in the apo form and Ca^{2+} bound form, compared to the DREAM WT, pointing towards increased accessibility of the hydrophobic sites in the chimeric variant.

Table 4.1: Dissociation constants and Hill coefficients for 1,8 ANS binding to DREAM-NCS1 and DREAM WT.

	K_D (μM)	n
Apo DREAM-WT	195 ±20	1.1±0.1
Apo DREAM-NCS 1	32±2	1.9±0.1
Ca^{2+} DREAM-WT	62 ± 4	1.1±0.1
Ca^{2+} DREAM-NCS 1	22 ±4	1.3±0.2

4.5 Fluorescence lifetime of Trp169

Lifetime decay parameters for the Trp 169 residue were determined using a frequency domain approach and the plot of the phase shift and modulation ratio as a function of

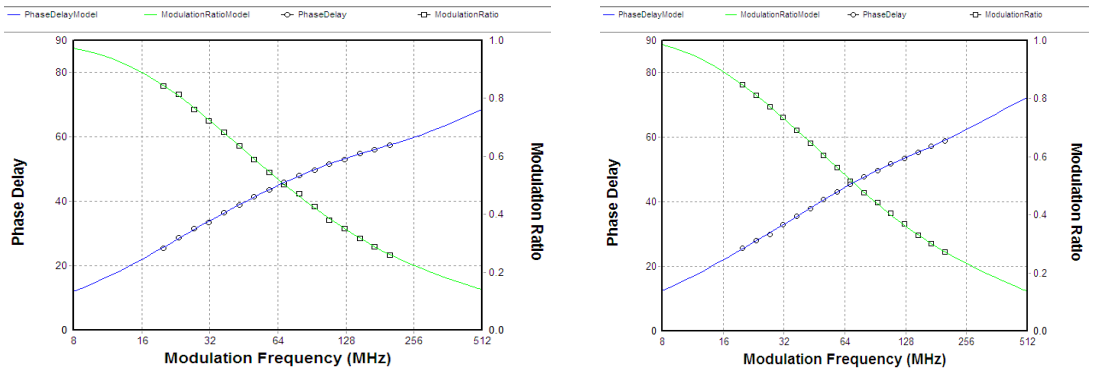

Fig. 4.8: Frequency domain Trp intensity decay for apo DREAM-NCS 1(left) and Ca^{2+} bound DREAM-NCs 1 (right). The solid lines correspond to the fit of the experimental data using a sum of three exponential decay model

modulation frequency is shown in Fig. 4.8. The curves were analyzed using sum of three exponential decay model and the decay parameters are summarized in Table 4.2 for

Table 4.2: : Emission decay parameters for DREAM WT and DREAM-NCS 1 in the presence and absence of Ca^{2+} and Mg^{2+}.

	Average lifetime (ns)	τ_1 (ns)	τ_2 (ns)	τ_3(ns)	α_1	α_2	α_3	χ^2
Apo DREAM WT	3.69	0.39± 0.03	2.28 ± 0.1	6.6 ± 0.3	0.29	0.29	0.29	4.38
Ca^{2+}DREAM WT	4.07	0.47± 0.02	2.57 ± 0.01	7.3 ± 0.3	0.29	0.19	0.05	2.93
Mg^{2+}DREAMWT	4.95	0.13 ± 0.01	1.22 ± 0.08	10.1 ± 0.3	1.85	0.15	0.04	3.105
Apo DREAMNCS 1	4.42	0.42± 0.05	2.15± 0.2	6.36± 0.3	0.29	0.14	0.09	0.91
Ca^{2+}DREAMNCS 1	4.81	0.58± 0.03	2.78± 0.2	8.11± 0.7	0.27	0.16	0.05	0.75
Mg^{2+}DREAMNCS1	3.87	0.48±0 .04	2.14± 0.3	5.87± 0.3	0.34	0.14	0.09	0.98

DREAM-NCS-1 and DREAM-WT in the presence and absence of divalent metal.

To provide additional information about the changes in the hydrophobic cavities on the protein surface, I have determined the lifetime of 1,8-ANS bound to DREAM-NCS 1 in the presence and the absence of Ca^{2+} using frequency domain approach. The data were

Table 4.3: Decay parameters for 1,8 ANS –DREAM WT and 1,8 ANS- DREAM-NCS 1 complex in the presence and absence of Ca^{2+}.The data were analyzed using a three exponential decay model. The data for DREAM WT are from Ref. Gonzalez and Miksovska, 2014.

	τ_1 (ns)	τ_2 (ns)	α_1	α_2	χ^2
1,8 ANS Apo DREAM WT	5.9± 0.1	16.2 ± 0.7	0.13	0.23	1.16
1,8 ANS Ca^{2+}DREAM WT	5.9± 0.2	17.6 ± 0.5	0.18	0.42	1.13
1,8 ANS Apo DREAM-NCS1	4.72± 0.2	16.5± 0.3	0.05	0.04	2.31
1,8 ANS Ca^{2+}DREAM-NCS 1	4.40± 0.2	16.4± 0.3	0.04	0.04	1.98

analyzed using a sum of three discreet exponential decays and the decay parameters are provided in Table 4.3.. The lifetime of 1,8-ANS unbound to protein was fixed to 0.27 (Gonzalez & Miksovska, 2014). The decay parameters for 1,8 ANS- DREAM WT were previously determined (Gonzalez & Miksovska, 2014) and are listed for the comparison. Interestingly, the lifetimes τ_1 and τ_2 are similar for both the WT and the mutant, suggesting that the binding sites for 1,8-ANS are identical in DREAM WT and DREAM-NCS-1.

Site 1 and site 2 interactions with DREAM-NCS 1

Previous data shown that binding of peptides mimicking the DREAM binding site 1 and site 2 in the T1 domain of K_v channel DREAM is regulated by Ca^{2+} and the affinity of DREAM for site 1 and site 2 increases approximately 25 and 50 times, respectively (Gonzalez and Miksovska, 2014).

Site 1 and site 2 interactions with DREAM-NCS were monitored by measuring the change in anisotropy upon DREAM-NCS 1 addition to peptides with a FITC fluorescent probe covalently attached to the N- terminus in the presence and absence of Ca^{2+}. Increase in the

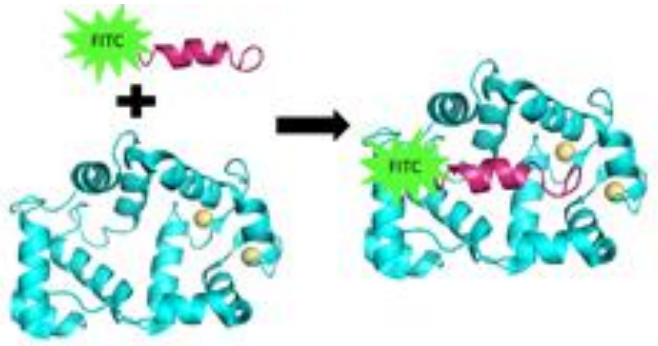

Fig. 4.9: Cartoon presentation of the interactions between FITC labeled site 1 (shown in purple) and DREAM (shown in light blue). Ca^{2+} ions are shown in yellow.

size of the FITC-labeled peptide upon complexation with DREAM protein (see Scheme 4.1) results in the increase in the anisotropy. Thus monitoring an increase in anisotropy as a function of the increased concentration of DREAM provides a convenient way determine the affinity of DREAM for individual peptides.

The titration curves for site 2 and site 1 binding to DREAM-NCS-1 in the absence and presence of Ca^{2+} are shown in Fig. 4.10 and Fig. 4.11, respectively. For both sites, the

anisotropy increases upon protein addition, suggesting that the chimeric protein binds both peptide. Analysis of titration curves using a quadratic equation as described in Material and Method section, provided equilibrium dissociation constants that are listed in Table 4.4.

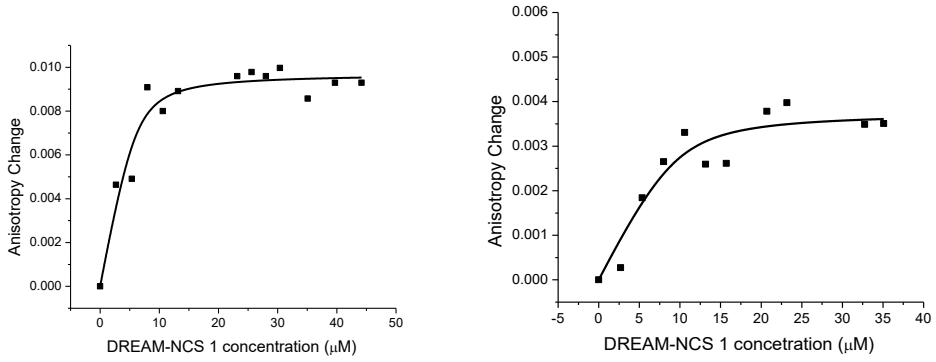

Fig. 4.10: Increase in anisotropy for Site 2 titration with DREAM –NCS 1 in the presence (left) and absence (right) of Ca^{2+}. The solid line corresponds to the fit of the experimental data using quadratic equation (Eq. 2.5)

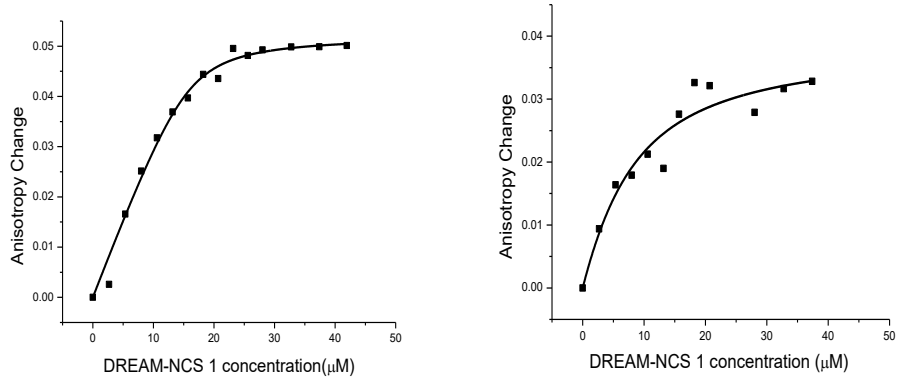

Fig. 4.11: Increase in anisotropy for Site 1 titration with DREAM –NCS 1 in the presence (left) and absence (right) of Ca^{2+}. The solid line corresponds to the fit of the experimental data using quadratic equation (Eq. 2.5)

Table 4.4: Dissociation constant for DREAM-NCS 1 interactions with Site 1 and Site 2 peptides , in the presence and absence of Ca^{2+}.

	K_D (μM)
Apo DREAM-NCS 1- Site 1	13.7 ±0.8
Apo DREAM-NCS 1 – Site 2	3.9±0.60
Ca^{2+} DREAM-NCS 1 Site 1	7.9 ± 0.8
Ca^{2+} DREAM-NCS 1 Site 2	9.0 ± 1.9

The equilibrium dissociation constants determined for site 1 and site 2 binding to DREAM-NCS-1 chimeric variant show an increased affinity compared to DREAM WT data and more importantly, the affinity for site 1 and site 2 is only weakly influenced by the presence of Ca^{2+} as the affinity for site 1 increases only two times in the presence of Ca^{2+} whereas affinity of Ca^{2+} bound DREAM-NCS-1 is approximately 2.5 weaker in the presence of Ca^{2+} compared to the metal free protein.

4.6 Discussion

Here we present the characterization of structural and functional properties of the chimeric DREAM-NCS-1. The Trp 169 emission spectra indicate that the replacement of Leu residues by Ser and Thr as well as modification of the loop between EF-hand 3 and EF-hand 4 strongly impact the Trp 169 surrounding as the emission spectra are red shifted, likely due to the more polar environment of the intrinsic probe. The different transition

upon Ca^{2+} binding to apoDREAM-NCS-1 compared to DREAM WT was observed, i.e. increase in the emission intensity, indicating distinct changes in the tertiary structure of the chimeric protein in the presence of Ca^{2+}. Interestingly, similar increase in the emission intensity upon Ca^{2+} association was observed previously for Ca^{2+} binding to NCS-1 (Aravind et al., 2008) (Aravid et al, 2008)[JM8],suggesting that photo-physical properties of Trp 169 in the chimeric protein resemble to those observed for NCS-1, at least in the presence of Ca^{2+}. However, the Trp 169 lifetime data determined for the chimeric DREAM-NCS-1 f or DREAM-WT suggest similar dynamic properties of Trp 169 and its surrounding in both proteins. The CD data clearly demonstrate that despite the red shift in the Trp emission spectrum, the chimeric protein has similar secondary structure DREAM WT and thus the absence of Leu 158 and Leu 159 residues as well as substitution of residues in the loop connecting EF-hand 3 and EF-hand 4 did not perturbed the proteins structure. The emission spectra of 1,8-ANS probe bound to apo DREAM-NCS-1 and Ca^{2+} bound DREAM-NCS-1 (λ_{max} = 471 nm and 491 nm, respectively) are red shifted with respect to the maxima of 1,8-ANS bound apoDREAM WT and 1,8-ANS bound Ca^{2+}DREAM (λ_{max} = 461 for both adducts, Gonzalez and Miksovska, 2014), suggesting that hydrophobic cavities are somewhat more polar in the chimeric protein. In addition, the affinity of the dimeric protein for 1,8-ANS increases 6 times and 3 times in the absence and presence of Ca^{2+}, respectively. We associate the increase in the affinity for a,8-ANS with the absence of the tetrameric and dimeric state in the apo and Ca^{2+} bound form of DREAM-NCS-1 due to the increased accessibility of the hydrophobic cavities.

The chimeric version of the protein interacts more closely with the peptides mimicking the site 1 and site 2 binding sites in the Kv channel T1 domain. Analogously with the increased

affinity for 1,8-ANS, these data indicates increased accessibility of the site1 and site2 binding sites on the protein surface due to the lack of the apoDREAM-NCS-1 tetramer and Ca^{2+}DREAM-NCS-1 dimer. Interestingly, Ca^{2+} regulated increase affinity of DREAM WT for site 1 and site 2 is not observed in this construct, suggesting, that the presence of the dimeric form is necessary for Ca^{2+} regulation of DREAM affinity for site 1 and site 2 binding sites.

Although these data points towards a distinct oligomerization form of chimeric DREAM-NCS-1 protein, additional experiments, that directly monitor the changes in protein oligomerization, such as dynamic light scattering, are necessary to confirm the above results. Also, molecular dynamic studies will provide insight into the distinct structural properties of DREAM-NCS-1.

LIST OF REFERENCES

Ames, J. B. (2018). Dimerization of neuronal calcium sensor proteins. *Frontiers in Molecular Neuroscience, 11*, 397. doi:10.3389/fnmol.2018.00397

Ames, J. B., & Lim, S. (2012). Molecular structure and target recognition of neuronal calcium sensor proteins. *BBA - General Subjects, 1820*(8), 1205-1213. doi:10.1016/j.bbagen.2011.10.003

Aravind, P., Chandra, K., Reddy, P. P., Jeromin, A., Chary, K. V. R., & Sharma, Y. (2008). Regulatory and structural EF-hand motifs of neuronal calcium sensor-1: Mg2+ modulates Ca2+ binding, Ca2+-induced conformational changes, and equilibrium unfolding transitions. *Journal of Molecular Biology, 376*(4), 1100-1115. doi:10.1016/j.jmb.2007.12.033

Azam, S., & Miksovska, J. (2019). Pb2+ binds to downstream regulatory element antagonist modulator (DREAM) and modulates its interactions with binding partners: A link between neuronal calcium sensors and Pb2+ neurotoxicity. *ACS Chemical Neuroscience, 10*(3), 1263-1272. doi:10.1021/acschemneuro.8b00335

Bähring, R. (2018). Kv channel-interacting proteins as neuronal and non-neuronal calcium sensors. *Channels, 12*(1), 187-200. doi:10.1080/19336950.2018.1491243

Braunewell, K. H., Spilker, C., Behnisch, T., & Gundelfinger, E. D. (1997). The neuronal calcium-sensor protein VILIP modulates cyclic AMP accumulation in stably transfected C6 glioma cells: Amino-terminal myristoylation determines functional activity. *Journal of Neurochemistry, 68*(5), 2129-2139. doi:10.1046/j.1471-4159.1997.68052129.x

Braunewell, K., & Gundelfinger, E. D. (1999). Intracellular neuronal calcium sensor proteins: A family of EF-hand calcium-binding proteins in search of a function. *Cell & Tissue Research, 295*(1), 1-12. doi:10.1007/s004410051207

Burgoyne, R. D., & Weiss, J. L. (2001). The neuronal calcium sensor family of Ca2+-binding proteins (vol 353, pg 1, 2001). *Biochemical Journal, 354*, 727. doi:10.1042/0264-6021:3540727v

Burgoyne, R. D., & Haynes, L. P. (2012). Understanding the physiological roles of the neuronal calcium sensor proteins. *Molecular Brain, 5*(1), 2. doi:10.1186/1756-6606-5-2

Calvert, P. D., Klenchin, V. A., & Bownds, M. D. (1995). Rhodopsin kinase inhibition by recoverin. function of recoverin myristoylation. *The Journal of Biological Chemistry, 270*(41), 24127-24129. doi:10.1074/jbc.270.41.24127

Carrión, A. M., Link, W. A., Ledo, F., Mellström, B., & Naranjo, J. R. (1999). DREAM is a Ca2+-regulated transcriptional repressor. *Nature, 398*(6722), 80-84. doi:10.1038/18044

Chazin, W. J. (2011). Relating form and function of EF-hand calcium binding proteins. *Accounts of Chemical Research, 44*(3), 171-179. doi:10.1021/ar100110d

Cheng, H. M., & Penninger, J. M. (2004). DREAMing about arthritic pain. *Annals of the Rheumatic Diseases, 63*(suppl 2), ii72-ii75. doi:10.1136/ard.2004.029942

Dason, J., Romero-Pozuelo, J., Atwood, H., & Ferrús, A. (2012). Multiple roles for frequenin/NCS-1 in synaptic function and development. *Molecular Neurobiology, 45*(2), 388-402. doi:10.1007/s12035-012-8250-4

Dong, Z., Saikumar, P., Weinberg, J. M., & Venkatachalam, M. A. (2006). Calcium in cell injury and death. *Annual Review of Pathology-Mechanisms of Disease, 1*(1), 405-434. doi:10.1146/annurev.pathol.1.110304.100218

Findeisen, F., Hura, G. L., Minor, D. L., & Pioletti, M. (2006). Three-dimensional structure of the KChIP1-Kv4.3 T1 complex reveals a cross-shaped octamer. *Nature Structural & Molecular Biology, 13*(11), 987-995. doi:10.1038/nsmb1164

Gasymov, O. K., & Glasgow, B. J. (2007). ANS fluorescence: Potential to augment the identification of the external binding sites of proteins. *BBA - Proteins and Proteomics, 1774*(3), 403-411. doi:10.1016/j.bbapap.2007.01.002

Gifford, J. L., Walsh, M. P., & Vogel, H. J. (2007). Structures and metal-ion-binding properties of the Ca2+-binding helix–loop–helix EF-hand motifs. *The Biochemical Journal, 405*(2), 199-221. doi:10.1042/BJ20070255

Gonzalez, W. G., & Miksovska, J. (2014). Application of ANS fluorescent probes to identify hydrophobic sites on the surface of DREAM. *BBA - Proteins and Proteomics, 1844*(9), 1472-1480. doi:10.1016/j.bbapap.2014.05.004

Greenfield, N. J. (2007). Using circular dichroism spectra to estimate protein secondary structure. *Nature Protocols, 1*(6), 2876-2890. doi:10.1038/nprot.2006.202

Jameson, D. M. (2014). *Introduction to fluorescence*. Boca Raton, FL: CRC Press. doi:10.1201/b16502

Lakowicz, J. R. (2006). *Principles of fluorescence spectroscopy*. Boston: Springer. doi:10.1007/978-0-387-46312-4

Li, C., Pan, W., Braunewell, K. H., & Ames, J. B. (2011). Structural analysis of Mg2+and Ca2+Binding, myristoylation, and dimerization of the neuronal calcium sensor and visinin-like protein 1 (VILIP-1). *The Journal of Biological Chemistry, 286*(8), 6354-6366. doi:10.1074/jbc.M110.173724

Lilliehook, C., Buxbaum, J. D., Wasco, W., Merriam, D. E., Luo, Y., Crowley, A. C., & Choi, E. (1998). Calsenilin: A calcium-binding protein that interacts with the presenilins and regulates the levels of a presenilin fragment. *Nature Medicine, 4*(10), 1177-1181. doi:10.1038/2673

Ling, H., Hinson, J. W., Cao, J., Betty, M., Mattsson, K. I., An, W. F., . . . Bowlby, M. R. (2000). Modulation of A-type potassium channels by a family of calcium sensors. *Nature, 403*(6769), 553-556. doi:10.1038/35000592

Lock, J. T., Smith, I. F., & Parker, I. (2019). Spatial-temporal patterning of Ca2+ signals by the subcellular distribution of IP3 and IP3 receptors. *Seminars in Cell and Developmental Biology, 94*, 3-10. doi:10.1016/j.semcdb.2019.01.012

López-Hurtado, A., Burgos, D. F., González, P., Dopazo, X. M., González, V., Rábano, A., . . . Naranjo, J. R. (2018). Inhibition of DREAM-ATF6 interaction delays onset of cognition deficit in a mouse model of huntington's disease. *Molecular Brain, 11*(1), 1-8. doi:10.1186/s13041-018-0359-6

Lusin, J. D., Vanarotti, M., Li, C., Valiveti, A., & Ames, J. B. (2008). NMR structure of DREAM: Implications for Ca2+-dependent DNA binding and protein dimerization. *Biochemistry, 47*(8), 2252-2264. doi:10.1021/bi7017267

Maret, W., & Li, Y. (2009). Coordination dynamics of zinc in proteins. *Chemical Reviews, 109*(10), 4682-4707. doi:10.1021/cr800556u

Martinez, J. C., Murciano-Calles, J., Cobos, E. S., Iglesias-Bexiga, M., Luque, I., & Ruiz-Sanz, J. (Eds.). (2013). *Isothermal titration calorimetry: Thermodynamic analysis of the binding thermograms of molecular recognition events by using equilibrium models.* InTech. doi:10.5772/53311

Masanori Osawa, Alexandra Dace, Kit I. Tong, Aswani Valiveti, Mitsuhiko Ikura, & James B. Ames. (2005). Mg2+ and Ca2+ differentially regulate DNA binding and dimerization of DREAM. *Journal of Biological Chemistry, 280*(18), 18008-18014. doi:10.1074/jbc.M500338200

Myers, W. K., Xu, X., Li, C., Lagerstedt, J. O., Budamagunta, M. S., Voss, J. C., . . . Ames, J. B. (2013). Double Electron–Electron resonance probes Ca2+-induced

conformational changes and dimerization of recoverin. *Biochemistry, 52*(34), 5800-5808. doi:10.1021/bi400538w

Ooi, L., & Wood, I. C. (2008). Regulation of gene expression in the nervous system. *The Biochemical Journal, 414*(3), 327-341. doi:10.1042/BJ20080963

Pandalaneni, S., Karuppiah, V., Saleem, M., Haynes, L. P., Burgoyne, R. D., Mayans, O., . . . Lian, L. (2015). Neuronal calcium sensor-1 binds the D2 dopamine receptor and G-protein-coupled receptor kinase 1 (GRK1) peptides using different modes of interactions. *The Journal of Biological Chemistry, 290*(30), 18744-18756. doi:10.1074/jbc.M114.627059

Permyakov, E. A., & Kretsinger, R. H. (2011). *Calcium binding proteins* (1st ed.). Hoboken, NJ: John Wiley & Sons.

Permyakov, S. E., Cherskaya, A. M., Wasserman, L. A., Khokhlova, T. I., Senin, I. I., Zargarov, A. A., . . . Permyakov, E. A. (2003). Recoverin is a zinc-binding protein. *Journal of Proteome Research, 2*(1), 51-57. doi:10.1021/pr025553i

Ping Liang, Huayi Wang, Hao Chen, Yuanyuan Cui, Lichuan Gu, Jijie Chai, & KeWei Wang. (2009). Structural insights into KChIP4a modulation of Kv4.3 inactivation. *Journal of Biological Chemistry, 284*(8), 4960-4967. doi:10.1074/jbc.M807704200

Plum, L. M., Rink, L., & Haase, H. (2010). The essential toxin: Impact of zinc on human health. *International Journal of Environmental Research and Public Health, 7*(4), 1342-1365. doi:10.3390/ijerph7041342

Pongs, O., Lindemeier, J., Zhu, X. R., Theil, T., Engelkamp, D., Krah-Jentgens, I., . . . Ferrús, A. (1993). Frequenin—A novel calcium-binding protein that modulates synaptic efficacy in the drosophila nervous system. *Neuron, 11*(1), 15-28. doi:10.1016/0896-6273(93)90267-U

Ramirez, D., Gonzalez, W., Fissore, R. A., & Carvacho, I. (2017). Conotoxins as tools to understand the physiological function of voltage-gated calcium (ca-V) channels. *Marine Drugs, 15*(10), 313. doi:10.3390/md15100313

Smith, T. F., & Waterman, M. S. (1981). Identification of common molecular subsequences. *Journal of Molecular Biology, 147*(1), 195-197. doi:10.1016/0022-2836(81)90087-5

Stryer, L. (1965). The interaction of a naphthalene dye with apomyoglobin and apohemoglobin. A fluorescent probe of non-polar binding sites. *Journal of Molecular Biology, 13*(2), 482. doi:10.1016/S0022-2836(65)80111-5

Vallee, B. L., & Falchuk, K. H. (1993). The biochemical basis of zinc physiology. *Physiological Reviews, 73*(1), 79-118. doi:10.1152/physrev.1993.73.1.79

Warren, J. T., Guo, Q., & Tang, W. (2007). A 1.3Å structure of zinc-bound N-terminal domain of calmodulin elucidates potential early ion-binding step. *Journal of Molecular Biology, 374*(2), 517-527. doi:10.1016/j.jmb.2007.09.048

Wei, Y., Thyparambil, A. A., & Latour, R. A. (2014). Protein helical structure determination using CD spectroscopy for solutions with strong background absorbance from 190-230 nm. *Biochimica Et Biophysica Acta, 1844*(12), 2331-2337. doi:10.1016/j.bbapap.2014.10.001

Yu, L., Sun, C., Mendoza, R., Wang, J., Matayoshi, E. D., Hebert, E., . . . Olejniczak, E. T. (2007). Solution structure and calcium-binding properties of EF-hands 3 and 4 of calsenilin. *Protein Science, 16*(11), 2502-2509. doi:10.1110/ps.072928007